

This manuscript is a preprint and has been submitted for publication in Basin Research. Please note that the manuscript has not yet undergone peer-review and is yet to be accepted for publication. Subsequent versions of this manuscript may have slightly different content. If accepted, the final version of this manuscript will be available via the 'Peer-reviewed Publication DOI' link on the right-hand side of this webpage. Please feel free to contact the authors with any comments, we welcome feedback.

2 **Running Head:** Cretaceous mixed-system, Azerbaijan

3 **Title: Evolution of a mixed siliciclastic-carbonate deep-marine system on an**
4 **unstable margin: the Cretaceous of the Eastern Greater Caucasus, Azerbaijan**

5

6

7 **Authors:** ZOË A. CUMBERPATCH^{1*}, EUAN L. SOUTTER¹, IAN A. KANE¹ and MAX
8 CASSON¹

9

10

11 **Institutions:**

12 ¹Department of Earth and Environmental Sciences, University of Manchester, Oxford Road

13

14

15 **Email:** zoe.cumberpatch@manchester.ac.uk

16

17

18 **Keywords:** deep-marine, mixed-system, siliciclastic-carbonate, Caucasus, Azerbaijan,

ABSTRACT

Mixed siliciclastic-carbonate deep-marine systems, herein termed ‘mixed systems’, are less well documented than their siliciclastic-dominated counterparts, but may be common globally and misinterpreted as transient transition zones between carbonate and siliciclastic deposition. The well-exposed Upper Cretaceous mixed-system of the Buduq Trough, Eastern Greater Caucasus (EGC), Azerbaijan, provides an opportunity to study the interaction between contemporaneous siliciclastic and carbonate deep-marine deposition. The Buduq Trough represents a sub-basin formed within the larger unstable post-rift margin of the EGC. Qualitative and quantitative facies analysis reveals that Upper Cretaceous stratigraphy of the Buduq Trough comprises a Cenomanian-Turonian siliciclastic submarine channel complex, which abruptly transitions into a Coniacian-Maastrichtian mixed-lobe succession. The Cenomanian – Turonian channels are shown to be entrenched in lows on the palaeo-seafloor, with the sequence entirely absent 10 km toward the west, where a Lower Cretaceous submarine landslide complex is suggested to have acted as a topographic barrier to deposition. By the Campanian this topography was largely healed, allowing deposition of the mixed-lobe succession across the Buduq Trough. Evidence for topography remains recorded through opposing palaeocurrents and frequent submarine landslides. The overall sequence is interpreted to represent abrupt Cenomanian-Turonian siliciclastic progradation, followed by ~Coniacian retrogradation, before a more gradual progradation in the Santonian-Maastrichtian. This deep-marine siliciclastic system interfingers with a calcareous system from the Coniacian onwards. These mixed lobe systems are different to siliciclastic-dominated systems in that they contain both siliciclastic and calcareous depositional elements, making classification of distal and proximal difficult using conventional terminology and complicating palaeogeographic interpretations. Modulation and remobilisation also occurs between the two contemporaneous systems, making stacking patterns difficult to decipher. The Buduq Trough is analogous in many ways to offshore The Gambia, NW Africa, and could be a suitable analogue for mixed deep-marine systems globally.

Introduction

Mixed siliciclastic-carbonate systems

Sedimentary successions characterised by contemporaneous deposition of both siliciclastic and carbonate lithologies, herein termed ‘mixed-systems’, have been identified from the Cambrian (Osleger and Montañez, 1996) to the Quaternary (Dunbar & Dickens, 2003; Tucker, 2003). Mixed systems are formed by a variety of depositional processes (e.g. Mount, 1984; Chiarella et al. 2017) and are consequently recognised in a variety of depositional environments, such as: shoreface (Zonneveld et al. 1997), lagoonal (Mitchell et al. 2001), shelfal (Mount, 1984; Zeller et al. 2015), slope (Gawthorpe, 1986) and (Ditty et al. 1997; Yose & Heller, 1989; Bell et al. 2018; Moscardelli et al. 2019). Mixed-systems deposited in deep-marine (below storm-wave base) are usually formed by material shed from a shallower carbonate-producing shelf that periodically received terrigenous sediment (Fig. 1) (Mount, 1984; Dunbar & Dickens, 2003; Crevello & Schlager, 1980). This material is then re-deposited in deep-marine by a spectrum of sediment gravity flows types, from turbidity currents to submarine landslides (Dorsey & Kidwell, 1999; Miller & Heller, 1994; Tassy et al. 2015; Moscardelli et al. 2019).

62 *Mixed lobes*

63

64 Sediment-gravity-flows that lose confinement on the slope or basin-floor build lobate depositional
65 bodies, known as lobes, which form important archives of palaeoclimatic and palaeogeographic
66 information (e.g. Hessler & Fildani, 2019). Exhumed deep-marine lobes have been studied in great
67 detail, and a wide variety of stacking patterns, depositional processes and facies distributions have
68 been described and interpreted (e.g. Mutti, 1983; Postma et al. 1993; Pr lat et al. 2009; Terlaky et
69 al. 2016; Kane et al. 2017; Bell et al. 2018; Fildani et al. 2018; Fonnesu et al. 2018; Soutter et al.
70 2019, Cumberpatch et al. in prep.). These studies typically focus on siliciclastic systems, with few
71 studies investigating the characteristics of lobes formed in mixed-systems (Fig. 1). This study aims
72 to address this by describing exhumed Cretaceous submarine lobes from the Eastern Greater
73 Caucasus (EGC), Azerbaijan (Fig. 2) which were built by contemporaneous deposition of
74 calcareous and siliciclastic sediment gravity flows. The characteristics of these mixed lobes and the
75 processes that govern their deposition are then compared with siliciclastic lobes. This study will
76 also describe the sedimentological evolution of the basin throughout the Cretaceous, providing
77 insights into the stratigraphic evolution of a basin characterised by unstable margins.

78

Geological Setting and Basin Structure

79

Evolution of the Eastern Greater Caucasus

80

81 The Eastern Greater Caucasus forms the easternmost extent of the NW-SE trending Greater
82 Caucasus orogenic belt, which runs from the Black Sea in the west to the Caspian Sea in the east
83 (Fig. 2) (e.g. Bochud 2011). The EGC sits on the southern-edge of the Scythian Platform, which
84 represents the southern margin of the Eastern European continent (Saintot et al. 2006). The
85 exposed EGC is mainly composed of Mesozoic-aged sediments that accumulated during multiple
86 phases of extension and convergence related to sequential closure of the Tethys toward the south
87 (Golonka, 2004; Vincent et al. 2007). Most of these Mesozoic tectonic events occurred in the
88 Jurassic, with Upper Triassic-Lower Jurassic compression followed by Lower- to Mid-Jurassic
89 rifting and compression, and Upper Jurassic rifting and compression (Bochud 2011). These
90 tectonic events are recorded by major thickness variations across the Middle Jurassic interval (Fig.
91 3).

92

93 The Lower Cretaceous of the EGC was deposited within an unstable marine environment, as
94 recorded by frequent mass-wasting events and major thickness changes across the interval (Egan
95 et al. 2009; Bochud 2011). Subsidence increased through the Lower Cretaceous and into the early
96 Upper Cretaceous due to back-arc extension associated with the opening of the West Black Sea
97 Basin to the west (Nikishin et al. 2001), resulting in deep-marine deposition of extensive
98 mudstones interspersed by submarine landslide deposits and terrigenous sediments (e.g. Brunet et
99 al. 2003).

100

101 The remainder of the Cretaceous sequence was deposited during a period of thermal subsidence
102 on a southward-dipping slope, with the basin divided into a series of sub-basins (Bochud 2011).
103 One of these sub-basins, the Buduq Trough, encompasses our study area. The Cretaceous
104 stratigraphy is dominated by calcareous and siliciclastic turbidites and conglomerates interbedded

105 with hemipelagic marls and mudstones (e.g. Brunet et al. 2003). A number of intra-Cretaceous
106 unconformities are seen within the basin and are related to periods of compression (Egan et al.
107 2009) or sea-level fluctuations. The end of the Cretaceous sequence is represented by a Base-
108 Cenozoic unconformity formed during Paleogene compression (Bochud 2011).

109

110 Collision of the Arabian and Eurasian plates in the Oligocene (Vincent et al. 2007) deformed the
111 Mesozoic and early Cenozoic succession into a series of exhumed synclines bound by major faults.
112 These faults separate distinct structural zones within the EGC (Fig. 2, Fig. 3) (Bochud 2011).

113

The Buduq Trough

114

115 The Buduq Trough is preserved in the east-west trending Qonaqkend structural zone (Fig. 4) and
116 has been interpreted as an Upper Cretaceous ‘paleo-valley’ incised into Lower Cretaceous deep-
117 marine sediments and Upper Jurassic limestones following a period of compression (Fig. 2B)
118 (Egan et al. 2009; Bochud 2011). It is likely that this compression was related to far-field tectonism
119 in the eastern Black Sea (Sosson et al. 2015), which overprinted the subsidence that characterised
120 the Cretaceous of the EGC. The earliest fill of the Buduq Trough is preserved in the east and is
121 represented by Cenomanian - Turonian sandstones and conglomerates (Fig. 2) (Bochud et al,
122 2011). The nature of this transition varies across and within the Trough; with the Cenomanian-
123 Turonian conformable with the Aptian-Albian at Mt. Kelevudag (Kopaevich et al. 2015) and sitting
124 directly on Barremian at Khirt (Fig. 2, Fig. 3). The overlying Coniacian-Maastrichtian is
125 represented by mixed siliciclastic-carbonate turbidites and is conformable with the Cenomanian-
126 Turonian in the west. In the east, near Cek, the Cenomanian-Turonian is absent, with the
127 Campanian directly overlying Aptian-Albian thin-bedded mudstones, submarine landslide deposits
128 and predominantly siliciclastic turbidites (Fig. 2, Fig. 3). Upper Cretaceous oceanic red beds
129 (CORBs) are also seen throughout the Upper Cretaceous sequence, particularly in the Coniacian
130 – Campanian turbidites and marls, indicating periodically oxic deep-marine conditions (e.g. Hu et
131 al. 2005).

132

Data and Methods

133 The data set comprises 23 sedimentary logs, totalling 500 m, collected across the Buduq Trough
134 (see supplementary material). Logs were generally collected at 1:25 scale. Bedding and structural
135 data (Fig. 4) and palaeocurrent data (Fig. 5) were collected to ground truth the geological map and
136 cross sections of Bochud (2011). Palaeocurrent readings were quite rare and were taken only where
137 sedimentary structures were clear enough to permit unambiguous data collection. Sparse
138 biostratigraphic data (Bochud 2011) hinders precise correlation across the study area. Chrono-
139 stratigraphic subdivision of the Buduq Trough are still being refined (cf. Bochud 2011; Bragina &
140 Bragin, 2015; Kopaevich et al. 2015), possibly due to the litho-stratigraphic similarities between
141 the units and the complex paleo-topography in which they were deposited (Egan et al. 2009).
142 Therefore we use mapped stratigraphic units (J₁, J₂, K₁, K₂ etc.) and lithostratigraphy to suggest
143 associated ages (Bochud 2011). Sedimentary logs were used to develop a lithofacies scheme (Fig.
144 6, Table 1) and facies associations (Fig. 7).

145 Over 10,000 sedimentological measurements (e.g. bed thickness, grain size, facies) were collected
146 and quantitatively analysed (see supplementary material). Stratigraphic logs were assigned one of

147 seven facies associations (Fig. 7) in order to quantitatively compare bed statistics across deep-marine
148 sub-environments (Fig. 8, 9, 10, 11).

149 **Results**

150 *Lithofacies*

151 Carbonate and siliciclastic lithofacies presented in Table 1 and Fig. 6 represent beds deposited by
152 individual events (event beds) and are classified based on outcrop observations. ‘Mud’ is used here
153 as a general term, for mixtures of clay, silt and organic fragments.

154 *Facies Associations*

155
156 Facies associations have been interpreted based on the dominant lithofacies (Fig. 6, Table
157 1) and architecture of a given succession and are subdivided into siliciclastic and mixed (carbonate
158 and siliciclastic) associations (Fig. 7). Facies associations FA1, FA2 and FA3 are Cenomanian-
159 Turonian and FA 4, FA 5, FA 6 and FA 7 are Coniacian-Maastrichtian (Bochud 2011). Facies
160 associations commonly used for lobes (Prélat et al. 2009; Spychala et al. 2017) and channels (Kane
161 & Hodgson, 2011; Hubbard et al. 2014) best fit our observations.

162 *Siliciclastic Facies Associations*

163 *FA 1: Lobe Fringe*

164 *Observations:* FA 1 is dominated by metre-scale packages of thin-bedded siliciclastic siltstones to
165 fine-grained sandstones with subordinate mudstones and medium-bedded siliciclastic sandstones
166 (Fig. 7A). Beds are laterally extensive for 100’s of metres and are commonly flat based and flat
167 topped, often showing normal-grading from fine sandstone to siltstone. Planar and convolute
168 laminations are observed in the upper part of many beds. Debrites, hybrid beds, conglomerates
169 and thick-bedded sandstones are absent.

170
171 *Interpretations:* Thin-bedded, structured sandstones are interpreted to be deposited from low-
172 concentration turbidity currents (Mutti et al. 1992; Jobe et al. 2012; Talling et al. 2012). The lack
173 of hybrid beds and the thin-bedded nature, lateral-extent, fine-grain size and lack of ripple-
174 stratification indicate deposition in a distal lobe fringe (Fig. 9) (Mutti 1977; Prélat et al. 2009; Marini
175 et al. 2015; Spychala et al, 2017).

176 *FA 2: Channel Axis*

177 *Observations:* FA 2 is composed of metre-scale thick-bedded medium-pebbly sandstones and
178 conglomerates with lesser medium-bedded sandstones and rare thin-bedded sandstones,
179 mudstones, debrites and hybrid beds (Fig. 7B). Within the Cenomanian-Turonian succession, FA
180 2 has the highest frequency of thick-bedded sandstones, conglomerates and bi-tripartite beds (Fig.
181 9). Conglomerates often grade normally into thick-bedded sandstones, commonly associated with
182 a grain size break, with coarse-granular sandstone grade often missing. Where conglomerates do
183 not grade into thick-bedded sandstones they are amalgamated or are less commonly separated by
184 thin beds of mudstone. Conglomerates are poorly-sorted, clast-supported and contain sub-angular
185 – sub-rounded clasts of limestone, sandstone and mudstone that often crudely grade from cobbles
186 to pebbles upwards (Fig. 11). Conglomerates also often contain disarticulated shelly fragments.
187 Sandstone and conglomerate bases are almost always erosional.

188 Thick-bedded sandstones are often normally-graded but can be non-graded or inversely-graded.
189 Decimetre scale mud-clasts are common throughout thick-bedded sandstones and low angle cross-
190 stratification is infrequently observed. Thin- to medium-bedded sandstones often have erosional
191 bases and contain convolute, hummock-like and planar laminations and are normally-graded, with
192 rare examples of inverse- or non- grading. These sandstones are either amalgamated or separated
193 by 10 cm thick mudstone layers, and often contain mud-clasts throughout the bed with granules
194 concentrated at the bed base. Sporadic debrites are also seen within FA 2; these have a deformed
195 mudstone matrix and contain clasts of limestone and sandstone. Hybrid beds are amalgamated
196 into 30-50 cm packages, with individual beds commonly consisting of a thin 2-4 cm fine-medium
197 grained sandstone overlain by a clast and shelly fragment rich 8-12 cm muddy very fine sandstone
198 debrite.
199 'Off-axis' successions have fewer thick-bedded sandstones and conglomerates than FA 2, but
200 more than FA 3, and fewer thin-medium, thick-bedded sandstones than FA 3, but more than FA
201 2 (Fig. 9).

202

203 *Interpretations:* The thick-bedded nature, coarse grain size, amalgamation, erosion and entrainment
204 of clasts within the sandstones suggests that the parent flows were highly energetic and capable of
205 eroding and bypassing sediment (Mutti 1992; Stevenson et al. 2015) and are thus these beds are
206 interpreted as high density turbidites (Lowe 1982). The poorly-sorted nature of the conglomerates
207 suggests that they were initially deposited by laminar flows (Sohn 2000), however apparent grading
208 of conglomerates into thick-bedded sandstones could reflect the transition of hyper-concentrated
209 submarine debris flows into highly-concentrated turbulent flows (Mulder and Alexander, 2001)
210 due to entrainment of ambient water (Postma et al. 1988; Kane et al. 2009).

211

212 The transition from conglomerates to medium-very coarse sandstone is associated with a grain
213 size break, often missing the granule fraction, suggesting bypass of flow (Stevenson et al. 2015).
214 The coarse-grain size and basal location of the conglomerates with respect to thick-bedded
215 sandstones suggests these beds could have been deposited as channel-base lags (Hubbard et al.
216 2014). Erosionally-based lenticular sandstones grading from cobble- to fine-sandstones are
217 interpreted to represent submarine channel fill (Jobe et al. 2017; Bell et al. 2018). This facies
218 association is consistent with gravelly-conglomeratic deposits reported elsewhere to represent
219 submarine channel axis deposition (Postma, 1984; Nemeč & Steel 1984; Surlyk 1984; Dickie &
220 Hein, 1995; Kane et al. 2009; Li et al. 2018; McArthur et al. 2019; Kneller et al. 2020).

221

222 While typically related to storm deposits (e.g. Hunter & Clifton, 1982), hummock-like cross-
223 lamination have been interpreted in deep marine environments elsewhere as anti-dune
224 stratification (Mulder et al. 2009), bottom current deposits (Basilici et al. 2012) and reworking of
225 an initial deposit by a subsequent flow (Mutti 1992; Tinterri et al. 2017). The channel axis
226 interpretation of FA 2 speculatively suggests anti-dunes formed by supercritical flows are the most
227 probable interpretation of these hummock-like structures (Araya & Masuda, 2001; Alexander,
228 2008).

229 *FA 3: Channel Margin*

230 *Observations:* FA 3 comprises thin-medium bedded fine-granular sandstones in 30-80 cm packages
231 interbedded with 10-90 cm dark mudstones (Fig. 7C). Within the siliciclastic Cenomanian-

232 Turonian succession FA 3 has the highest frequency of thin-medium bedded sandstones (Fig. 9).
233 Conglomerates and thick-bedded sandstones are rare in FA 3 (Fig. 9). Thin-bedded sandstones
234 and the upper part of medium-bedded sandstones can be argillaceous, with visible micaceous
235 grains and are often planar, ripple and convolute laminated, with rarer hummock-like laminations.
236 Sandstones are often normally-graded but inverse-grading is also observed. Beds of medium
237 thickness are rich in mud-clasts and commonly amalgamated along mud-clast laden surfaces, bases
238 can be highly erosive and scour-like, removing a significant proportion of the underlying bed.
239 Thin-bedded sandstones can be flat or erosively-based, commonly scoured; where bases are
240 erosional the lowermost part of the bed is commonly rich in granule-grade material (Fig. 7C).
241 Granules and coarser fragments are composed of limestone and sandstone. Infrequent hybrid beds
242 are composed of medium-coarse grained siliciclastic sandstone, overlain by a muddy, occasionally
243 marly fine sandstone debrite.

244
245 *Interpretations:* The thin-bedded nature and presence of tractional structures indicate that this facies
246 association was deposited by a low-density turbidity current (Lowe 1982). Presence of hummock-
247 like laminations could indicate storm-wave influenced deposition (Harms et al. 1975), however
248 their presence within a succession containing thick, dark mudstones and frequent sediment gravity
249 flows suggests a deep-marine origin. Anti-dune formation (Mulder et al. 2009) and tractional
250 reworking of an aggrading deposit (Mutti 1992; Tinterri et al. 2017; Bell et al. 2018) have both been
251 interpreted to form similar hummock-like lamination in deep marine environments. Clean
252 sandstones which grade into argillaceous, micaceous sandstones could indicate transitional flow
253 deposits (Sylvester & Lowe 2004; Baas et al. 2009; Kane & Pontén 2012). The thin-bedded, coarse
254 grain size and erosive nature of these deposits, along with the presence of supercritical bedforms,
255 is similar to the overbank deposits seen adjacent to bypass-dominated channels (Kane & Hodgson
256 2011; Hubbard et al. 2014; Jobe et al. 2017, Lin et al. 2018, McArthur et al. 2019). These similarities,
257 coupled with the along strike location of FA 3 adjacent to FA 2 (channel axis), has led to the
258 interpretation of FA 3 as a channel overbank (Fig. 9). The lateral transition of FA 2 and 3 is
259 indicative of 'on-axis' to 'off-axis' channel-belt facies (Kane et al. 2009).

261 *FA 4: Lobe Axis*

262 *Observations:* FA 4 is dominated by > 1 m thick packages of amalgamated conglomerates (Fig. 7D,
263 Fig. 9) interbedded with thin-thick bedded very fine - very coarse sandstones. Within the
264 Coniacian-Maastrichtian succession, the thickest conglomerates are found within FA4 (Fig. 8). The
265 conglomerates are laterally discontinuous, erosionally-based, and are either flat-topped when
266 onlapping, or convex-up when downlapping, the slope (Fig. 7, Fig. 12). Conglomerates increase in
267 frequency, clast size (up to cobble-grade) and thickness, up stratigraphy (Fig. 8) and contain sub-
268 angular to rounded clasts of limestone, sandstone and mudstone (Fig. 11). Within the Coniacian-
269 Maastrichtian stratigraphy the greatest number of amalgamated beds is in FA4 (Fig. 10) and the
270 largest grain size range (majority of beds between very-fine sandstone to medium grained
271 sandstone) is observed (Fig. 8). Within FA 4, a coarser grain size class (of coarse grained sandstone
272 or above) is observed which is almost absent in other Coniacian-Maastrichtian facies associations
273 (FA 5, FA 6, FA 7) (Fig. 8).

274

275 *Interpretations:* Amalgamation of event beds suggests parent flows were energetic and capable of
276 eroding sediment into the flow (Lowe 1982; Stevenson et al. 2015) and amalgamation of
277 conglomerates indicates deposition in a debris-flow dominated environment (Surlyk 1984; Postma
278 1984; Dickie & Hein, 1995), similar to the debris flow dominated lobes described by McHargue et
279 al. (2019). These conglomerates could also represent sediment bypass within lobe axes (e.g. Kane
280 et al. 2009) or channel fill conglomerates (e.g. Knaust et al. 2014), however their thickness, stacking
281 and geometry are most likely to represent deposition in the axis of a debris-flow dominated lobe.

282

Mixed Facies Associations

FA 5: Lobe Off-Axis

284 *Observations:* FA 5 is represented by erosively-based thin- to medium-bedded, fine-coarse grained
285 siliciclastic sandstones and thin- to medium-bedded fine-grained calcareous siltstones,
286 conglomerates and fine sandstones (Fig. 7E, Fig. 8). Sandstones with siliciclastic bases and
287 calcareous tops are present throughout and are often amalgamated with siliciclastic and calcareous
288 sandstones, forming packages separated by mudstones and silty-mudstones. Calcareous beds are
289 typically flat-based when overlying mudstones, whilst siliciclastic beds are commonly erosive.
290 Calcareous siltstones and sandstones are massive, whilst siliciclastic sandstones show planar,
291 convolute and ripple laminations, but can also be structureless. Debrites are interspersed, often
292 incorporating thin-bedded calcareous siltstones and sandstones. Hybrid beds are rare (Fig. 9).

293

294 *Interpretations:* The presence of both calcareous and siliciclastic sandstones suggests deposition in a
295 mixed system (Fig. 1, Fig. 10) (Al-Mashaikie & Mohammed, 2017; Chiarella et al. 2017; Walker et
296 al. 2019). Structureless medium-bedded calcareous siltstones and sandstones are interpreted to
297 represent deposition from medium density turbidity currents (Kneller & Branney 1995; Talling et
298 al. 2012; Soutter et al. 2019) aggrading quickly enough to prevent tractional sedimentary structure
299 development in their basal divisions (Kneller & Branney 1995; Sumner et al. 2008). This
300 depositional process is complicated within the calcareous medium-bedded deposits, which appear
301 to have aggraded much more slowly than their siliciclastic counterparts, as evidenced by thin-
302 bedded and medium-grained siliciclastic beds being deposited within medium-bedded and fine-
303 grained calcareous beds. The presence of medium-density turbidites, relatively coarse grain size
304 and common amalgamation suggests lobe off axis deposition (Prélat et al. 2009; Spychala et al.
305 2017).

FA 6: Proximal Fringe

307 *Observations:* Primarily composed of normally-graded, thin-medium bedded calcareous very-fine to
308 fine-grained sandstones and siltstones, with subordinate thin-bedded siliciclastic fine-medium
309 sandstones and mixed siliciclastic and calcareous sandstones (Fig. 7F, Fig. 8, Fig. 9). Calcareous
310 siltstones and sandstones are flat based when overlying mudstones, but are often erosive at
311 amalgamation surfaces (Fig. 10). Siliciclastic sandstones, either isolated or within mixed beds, are
312 frequently < 3 cm thick, with flat to weakly erosive bases (Fig. 6). Debrites are interspersed within
313 FA 6 and often rework the thin-bedded calcareous siltstones and sandstones. Planar laminations
314 are common within the thin-bedded siliciclastic and calcareous sandstones. Less common ripple
315 laminations show multiple and opposing palaeocurrent orientations. Hybrid beds are rare (Fig. 9).

316

317 *Interpretations:* The presence of both calcareous and siliciclastic sandstones suggests deposition in a
318 mixed system (Fig. 1, Fig. 10) (Al-Mashaikie & Mohammed, 2017; Chiarella et al. 2017; Walker et
319 al. 2019). Calcareous sandstones are interpreted to represent deposition from low- to medium-
320 density turbidity currents based on their bed thickness, fine grain size and structuration (Fig. 9)
321 (Lowe 1982; Mutti 1992). The thin-bedded siliciclastic sandstones could represent the depositional
322 products of flow transformation from up-dip debris flows (i.e. the up-dip conglomerates) to
323 turbulent flows following the entrainment of ambient water (Potsma 1988; Haughton et al. 2009),
324 which punctuate slowly aggrading calcareous turbidites, interpreted to represent the remnants of
325 dilute flows (Remacha & Fernández, 2003).

326
327 The preservation of both structured and structureless sandstones suggests an off-axis location of
328 deposition; similar preservation of both deposit types has been interpreted in the proximal lobe
329 fringe elsewhere (Prélat et al. 2009; Spsychala et al. 2017; Soutter et al. 2019). FA 6 is differentiated
330 from FA 5 based on its thinner beds and less frequent erosional events, and is therefore interpreted
331 as being more distal and deposited within the proximal fringe. Hybrid beds are rare throughout
332 the system therefore a distinction between frontal fringe and lateral fringe is difficult to decipher
333 (e.g. Spsychala et al. 2017).

334 *FA 7: Distal Fringe*

335 *Observations:* Dominated by laterally extensive, metre-scale packages of thin-bedded amalgamated
336 calcareous sandstones which are normally-graded from very fine – fine sandstone to siltstone and
337 are interbedded with metre-scale mudstones and silty-mudstones (Fig. 7G, Fig. 8, Fig. 9). Beds are
338 flat-based, flat-topped and frequently contain both parallel and convolute laminations. Medium-
339 bedded calcareous siltstones-fine sandstones are present, and may reflect amalgamated thinner-
340 beds which are difficult to decipher. Debrites, siliciclastic thin-bedded sandstones and hybrid beds
341 are rare (Fig. 9). The smallest grain size range (between siltstone and very-fine sandstone) is
342 observed in FA6 and FA7 (Fig. 8) and amalgamation is infrequent (Fig. 10). More thin beds are
343 seen in FA7 than elsewhere in stratigraphy (Fig. 7C, Fig. 8, Fig. 9).

344
345 *Interpretations:* Thin-bedded, structured sandstones are interpreted to be deposited from low-
346 concentration turbidity currents (Mutti et al. 1992; Jobe et al. 2012; Talling et al. 2012). The
347 presence of medium-bedded calcareous siltstones-fine sandstones and lack of ripple laminations
348 suggest slow aggradation from a turbulent flow (Remacha & Fernández 2003; Bell et al. 2018).
349 Lack of ripple lamination suggests flows did not reach significant velocity to generate ripple
350 laminations (Baas et al. 2016). The infrequency of hybrid beds and siliciclastic beds within this
351 facies association supports deposition within a carbonate dominated environment and the thin-
352 bedded nature, lateral-extent, fine-grain size and lack of ripple-stratification suggests deposition in
353 a distal lobe fringe (Mutti 1977; Prélat et al. 2009; Marini et al. 2015; Spsychala et al, 2017).

354 **Discussion**

355 *Nature of the Upper Cretaceous Topography*

356
357 Toward the west of the Qonaqkend Zone, Upper Cretaceous deep-marine sandstones and
358 limestones can be seen to thin towards, and onlap, Upper Jurassic limestones (Fig. 12, Fig. 13, Fig.

359 14). These Upper Jurassic limestones must therefore have formed 100s of metres of relief on the
360 Cretaceous seafloor. The most likely mechanism for the generation of seafloor topography is an
361 allochthonous block (Fig. 13, Fig. 14, Fig. 15). The presence of decametre-scale allochthonous blocks
362 (mega-clasts of Blair & McPherson 1999) and submarine landslide deposits throughout the
363 Cretaceous stratigraphy indicates a highly unstable margin, supporting this view (Fig. 13, Fig. 15).
364 The identification of a basin-scale submarine landslide deposit, which forms the Qizilqaya and
365 Shagdag mountains toward the west, further validates this interpretation (Bochud 2011) (Fig. 15)
366 with the mega-clasts in the west possibly forming part of this deposit (Fig. 14, Fig. 15, Fig. 16).
367 The contact is therefore formed as the Cretaceous stratigraphy infilled the accommodation present
368 on the irregular surface of the deposit. Such relationships have been observed at outcrop (e.g.
369 Burbank et al. 1992; Armitage et al. 2009, Kneller et al. 2018) and in the subsurface (Fig. 17) (e.g.
370 Soutter et al. 2018, Casson et al. 2020). Differential compaction around these rigid blocks will have
371 resulted in steepening of strata adjacent to the block, which may contribute to the gradual
372 steepening identified (Fig. 12, Fig. 14), which has been reported elsewhere (e.g. Burbank et al.
373 1992).

374

375 *Upper Cretaceous evolution of the Buduq Trough*

376

377 Deep-marine deposition within the Buduq Trough began following a period of compression and
378 folding in the mid-Cretaceous (Fig. 16) (Egan et al. 2009, Bochud 2011). Evidence of this
379 compression is seen within the earliest fill in the Trough, which is preserved toward the east of the
380 Qonaqkend structural zone. This early fill is represented by Cenomanian - Turonian conglomeratic
381 slope channels that either erode into Barremian deep-marine mudstones or sit conformably on
382 thin-bedded Aptian-Albian siliciclastic turbidites. These basal-Cenomanian stratigraphic
383 relationships are suggested to be caused by channels preferentially infilling lows present on
384 seafloor, forming entrenched channel axes that pinch-out laterally against Barremian mudstones
385 (Fig. 16). These lows may have formed during mid-Cretaceous compression and folding (Egan et
386 al. 2009; Sosson et al. 2016) or through submarine slope failure and consequent scour-formation.

387

388 It is possible that poorly preserved thin-bedded Aptian-Albian turbidites represent the distal
389 extents of the Cenomanian slope channels that were either eroded by the channels during
390 progradation or deposited within isolated lows on the Barremian slope. These lows may have
391 formed in response to similar processes to those which entrenched the Cenomanian channels. The
392 abrupt nature of the transition from distal fine-grained turbidite deposition to conglomeratic slope
393 channels may correspond to either tectonic rejuvenation during the Mid-Cretaceous
394 compressional event (Fig. 16) (Egan et al. 2009) and/or an abrupt relative sea-level fall, such as
395 the eustatic sea-level fall seen in the mid-Cenomanian (Miller et al. 2003).

396

397 Evidence for basinal topography is present during deposition of the Cenomanian – Turonian, with
398 the sequence almost entirely absent 10 km to the west at Cek, indicating the presence of a relative
399 high in this location. Submarine landslide thicknesses also increase toward this high in the
400 Barremian, suggesting the high influenced deposition from the Lower Cretaceous until the
401 Turonian. Previous work has shown the presence of a large Lower Cretaceous submarine landslide
402 toward the west (Fig. 16) (Bochud 2011), which is likely to form the high and the complex

403 stratigraphic relationships described previously (Fig. 13, Fig. 14, Fig. 15). It is also likely that this
404 submarine landslide, and other more minor ones in the area, were emplaced during an earlier
405 period of tectonism and instability related to Lower Cretaceous compression (Fig. 16). Evidence
406 for topography (Fig. 12) in the Late Cretaceous is also evident on a smaller scale through
407 paleocurrent reversals in low-density turbidites (e.g. Kneller et al. 1991) indicating a northward-
408 dipping slope confining southward-directed flows (Fig. 5, Fig. 12), and through the deposition of
409 Upper Jurassic blocks within the Turonian succession, indicating slope instability during this
410 period (Fig. 13, Fig. 15).

411
412 Following the Cenomanian-Turonian regression the Trough begins to deepen again during the
413 Coniacian-Maastrichtian (CM), as represented by the deposition of laterally-extensive, thin- to
414 medium-bedded, mixed-siliciclastic-carbonate turbidites overlying the slope channels (Fig. 16).
415 The mixed-lithology of the turbidites contrasts with the dominantly siliciclastic Aptian-Albian
416 turbidites underlying the slope channels, indicating a change in source or paleogeography between
417 the Lower and Upper Cretaceous (Fig. 5, Fig. 16). The presence of thinning and facies changes
418 toward present-day syncline margins, frequent debrites and out-runner blocks, and divergent
419 palaeocurrent distributions indicates that basinal topography had an impact on CM deposition
420 (Fig. 5, Fig. 12, Fig. 13, Fig. 15). This topography may have been formed by differential compaction
421 over the rigid limestone mega-clast, or external compression (Fig. 14, Fig. 15, Fig. 16). Erosional
422 contacts are seen within the CM succession at the base of small, metre-scale channel fills, which
423 occur with increasing frequency through time. These small channel fills are filled by conglomerates
424 and high-density turbidites with similar compositions to the underlying and much more extensive
425 slope channels. The channels are therefore interpreted as small distributary channels in the axes of
426 lobes that formed at the distal ends of the underlying slope channels (e.g. Normark et al. 1979).
427 The increasing frequency and thickness of these conglomerates through the CM (Fig. 8) may
428 therefore represent gradual progradation of the slope channels following their abrupt backstep at
429 the end of the Turonian. Clasts within these younger conglomerates are also more limestone-
430 dominated, which fits with the transition to a more carbonate-dominated system through the
431 Upper Cretaceous (Fig. 11, Fig. 16, Fig. 18).

432
433 Mixed-deep-marine deposition continues in the Buduq Trough throughout the remainder of the
434 Cretaceous until Palaeogene compression ceases deposition (Bochud 2011), forming an
435 unconformity between the Upper Cretaceous and overlying Palaeogene and Neogene sediments
436 (Fig. 2, Fig. 3).

437 *A Subsurface Analogue for the Buduq Trough*

438 A seismic-scale equivalent of a mixed-system analogous to the Cretaceous Buduq Trough has been
439 identified and is used to support and increase the resolution of our outcrop-based model. The
440 continental margin offshore The Gambia, NW Africa, developed through the Late Cretaceous
441 with remarkable similarities in timing and evolution to the Buduq Trough (summarised in Casson
442 et al. 2020 in press; Fig. 17). Unconfined mixed-systems developed on the deep-marine basin floor
443 are interpreted to have been line-fed through a heavily canyonised unconformity surface (Fig.
444 17C). Seismic geomorphology reveals the interfingering of siliciclastic-dominated and carbonate-

445 dominated systems (i.e. at X and Y Fig. 19), similar to that observed on facies and facies
446 architecture scale in the EGC (e.g. Fig. 6, Fig. 7).

447 Sediment gravity flows through the canyons eroded into the underlying carbonate platform
448 redepositing hundreds of metre-scale, seismically-resolvable carbonate mega-clasts 20+ km from
449 the escarpment (Fig. 17B, D); our field work suggests that these blocks may be associated with a
450 multitude of different types and sizes of submarine landslides and blocks that are below seismic
451 scale (Fig. 13, Fig. 15). The presence of carbonate blocks and lobe-architecture in the carbonate-
452 dominated systems (*sensu* McHargue et al. 2019) suggests deposition by debris-flows (i.e. FA 4).
453 Hence two stages of mixing occurs, firstly during erosion to form mixed lithology flows, and then
454 through deposition of interfingering systems. Pervasively channelised siliciclastic-systems with
455 single feeder channels show a distinct seismic geomorphological response to their carbonate
456 counterparts (Fig. 17D, E). The lateral location along the margin of siliciclastic-dominated systems
457 is conceivably related to sediment input points (i.e. shelf-incising canyons) capturing an extra-
458 basinal source of siliciclastic sediment from the shallow marine environment, away from shelfal
459 carbonate factories. Basin floor topography is created by early deposits and influences subsequent
460 lobe deposition (Fig. 17), causing stacking and lateral migration of lobes, which cannot be resolved
461 in the Buduq Trough (Fig. 18) probably because the scale of the study area is smaller than the scale
462 at which migration occurred.

463
464 Documentation of ancient subsurface mixed-systems has been achieved from the interpretation
465 of seismic reflection data (e.g. Moscardelli et al. 2019, Casson et al. 2020). It may also be possible
466 that transitions from calcareous-dominated to siliciclastic-dominated deep-marine systems, which
467 are commonly associated with the rapid arrival (progradation) of the siliciclastic system (e.g. Scott
468 et al. 2010; Kilhams et al. 2012; 2015; Soutter et al. 2019; Cumberpatch et al. in prep.), may have
469 been overlooked as ‘transition zones’, and in fact represent short-lived mixed systems, which are
470 often below the scale of seismic resolution. The role of mixed-system interactions on a grain-scale
471 and its implications in terms of reservoir quality remain unclear until such systems are drilled
472 (Chiarella et al. 2017; Bell et al. 2018; Moscardelli et al. 2019).

473 *Mixed lobes*

474 ***Lobe sub-environments:*** If individually observed, the siliciclastic system within the mixed
475 succession could be interpreted as stacked lobes with axial, off-axial and fringe sub-environments
476 identified. The calcareous system, however, would be interpreted as being predominantly lobe
477 fringe deposition (Remacha & Fernández 2003; Bell et al. 2018). Since the two systems are mixed
478 it is difficult to assign a single lobe sub-environment to a sequence of beds as they represent the
479 inter-fingering of two systems (Fig. 19). Due to the interaction of these systems, siliciclastic lobe
480 elements are likely to occur within calcareous lobe elements (Fig. 1, Fig. 17, Fig. 19) (Prélat et al.
481 2009), forming stacks of mixed event beds (D, Table 1). This is further complicated by often highly
482 erosive siliciclastic turbidity currents which can rework calcareous beds, as evidenced by calcareous
483 rip-up clasts within siliciclastic turbidites. This may remove individual calcareous lobe elements
484 from the rock record, and make stacking interpretations more difficult (Fig. 18) (Braga et al. 2001).

485
486 Due to these complexities it is perhaps necessary to refer to such systems with a more specific
487 descriptor (e.g. mixed axis-fringe), or broadly refer to them as ‘mixed systems’ in order to allude

488 to their complexity and contrast them from siliciclastic-dominated systems (Fig. 19). Use of the
489 siliciclastic lobe hierarchy of Prélat et al. (2009) is possible in mixed systems, but calcareous and
490 siliciclastic descriptors are required (Fig. 19). It is possible to decipher the different systems in our
491 field and subsurface examples, due to their lithological differences being visually resolvable at
492 outcrop (Fig. 6, Fig. 7) and showing different seismic characteristics in the subsurface (Fig. 17, Fig.
493 19). However, without detailed provenance and geochemical analysis it would be very difficult to
494 decipher the mixing of two siliciclastic systems or two calcareous systems, due to similarity in
495 depositional facies and thus seismic character. Unless an individual system can be followed from
496 source to sink in outcrop or the subsurface we must always consider the possibility of multiple
497 systems interacting, modulating each other and complicating stacking patterns (Fig. 19).

498

499 **Stacking patterns:** Deep-marine stacking motifs can show either aggradational, progradational,
500 retrogradational or unorganized stacking patterns (Stow & Mayall, 2000; Deptuck et al. 2007;
501 Straub et al. 2009; Prélat & Hodgson 2013), which can be modulated by both external and internal
502 processes (e.g. Ferguson et al. 2020). Our study shows that in mixed systems it can be difficult to
503 decipher stacking patterns within each individual system due to the convolution of each system by
504 the other (Fig. 18, Fig. 19). Bed thickness trends within the calcareous turbidites are difficult to
505 decipher, possibly due to their narrow grain size range preventing the identification of thinner-
506 beds, and amalgamation within thicker beds (Fig. 18).

507

508 Siliciclastic conglomerates become more frequent and thicker throughout the Coniacian-
509 Maastrichtian, perhaps reflecting a progradation of the siliciclastic system (Fig. 8, Fig. 16).
510 However, bed thickness and grain size analysis for the Coniacian-Maastrichtian do not show any
511 thickness trends or stacking patterns within the calcareous or siliciclastic turbidites (Fig. 18). This
512 suggests that in mixed systems it may therefore not be possible to describe the progradation or
513 retrogradation of an individual system, and only possible to describe the relative ratio between the
514 two; the apparent dominance of the mixed system (e.g. if siliciclastic (s) > carbonate (c) this could
515 be due to progradation of s or by the retrogradation of c, both of which are controlled by a number
516 of external and internal forcings).

517

518 On the scale of the outcrops (100s m), the calcareous turbidites appear to be sheet-like, while the
519 siliciclastic turbidites show thickness variation, representing more typical channel and lobe
520 geometries (e.g. Prélat et al. 2009). Conglomerates observed in the FA4 appear to be confined to
521 isolated depocentres and pinch-out across meters - 10s of meters, indicating the presence of subtle
522 topography (Fig. 12). This suggests the deposition of the conglomerates may have been controlled
523 by depositional topography (compensational stacking) and that the underlying calcareous
524 turbidites do exhibit subtle, long-wavelength thickness changes over a greater scale than observed
525 at outcrop, influencing subsequent sediment routing. Alternatively, the thinning of conglomerates
526 was due to the basinal topography present at this time, preventing these highly-concentrated flows
527 running-out over great distances (Fig. 12).

528

529 **Mixed-system origin:** Previous work on mixed systems has correlated alternations in calcareous
530 and siliciclastic turbidites to 3rd order sea level cycles (Yose & Heller, 1989; Miller & Heller, 1994);
531 the alternations in the Buduq Trough are lower frequency than these cycles but could be
532 interpreted as fifth-sixth order sea level cycles (parasequences) occurring on a 10,000 – 100,000

533 year cycle (Fig. 16) (Van Wagoner et al. 1990), related to Milankovitch orbital cycling
534 (Goldammer et al. 1990; D'Argenio et al. 1999). Elsewhere mixed systems have been interpreted
535 to represent alternating cool-wet and cold-dry climate cycles driven by precession orbital cycles
536 (García-García et al. 2009). No obvious stacking can be deduced in the study area (Fig. 18)
537 preventing a confident interpretation to be made regarding the forcings behind the high-frequency
538 lithological variations.

539
540 Rugose carbonate platform margins (e.g. Saller et al. 1989; Grant et al. 2019, Casson et al. 2020),
541 like those observed in the Buduq Trough (Fig. 13, Fig. 16, Fig. 17), have been proposed as conduits
542 for siliciclastics without requiring a sea level change (Francis et al. 2008; Braga et al. 2008; Puga-
543 Bernabéu et al. 2014; Al-Mashaikie & Mohammed, 2017; Walker et al. 2019). This could indicate
544 that the calcareous deep-marine system in the Buduq Trough is part of a much more extensive
545 and line-fed system derived from shedding of active carbonate factories perched on the shelf (e.g.
546 Fig. 17). The contemporaneous siliciclastic system may therefore have been derived from multiple
547 point source conduits along this margin that either 1) periodically punctuated this larger carbonate
548 system or 2) were long-lived conduits permanently bound by carbonate factories (Fig. 16) (Mueller
549 et al. 2017; Moscardelli et al. 2019). Two different sources for separate components of a mixed
550 system have been documented elsewhere (Fig. 1, Fig. 17, Fig. 19A) (Ditty et al. 1997; Riaz Ahmad
551 & Jamil Afzal, 2012; Poprawski et al. 2014; 2016; Chiarella et al. 2017). The presence of Late
552 Jurassic blocks (Fig. 13, Fig. 15) within the Cretaceous complicates this model, with the blocks
553 interpreted as either 1) Late Cretaceous failures from an exposed Jurassic shelf, 2) out-running
554 blocks from Lower Cretaceous failures (e.g. De Blasio et al. 2006) that were subsequently deposited
555 around during the Late Cretaceous, or 3) blocks that were periodically shed through the Late
556 Cretaceous from high-relief Lower Cretaceous slope submarine landslides identified in the west
557 (Fig. 14, Fig. 16).

558
559 Palaeoflow indicators are limited for the calcareous system due to lack of ripple lamination
560 developed in its fine-grained, slowly accumulating deposits (Baas et al. 2015). It is therefore
561 difficult to decipher whether these siliciclastic and calcareous systems were perpendicular, oblique
562 or parallel to each-other. The palaeoflow indicators that were collected, however, are consistent
563 with a provenance to the north (Fig. 5, Fig. 12, Fig. 15) A northern provenance is also suggested
564 from palaeographic maps for the interval, suggesting a Scythian platform source area (Nikishin et
565 al. 1998), and unpublished provenance data (Vincent, pers.comm.).

566 **Conclusion**

567
568 This study uses the Upper Cretaceous Buduq Trough, Azerbaijan to document the characteristics
569 of an unstable and mixed siliciclastic-carbonate system. Deposition in the Trough is represented
570 by a Cenomanian-Turonian submarine channel complex, which transitions into a Coniacian-
571 Maastrichtian mixed lobe succession. This sequence represents an abrupt Cenomanian regression,
572 probably related to a mid-Cretaceous compressional event and/or an abrupt mid-Cenomanian
573 eustatic sea level fall; followed by a relatively abrupt late Turonian-Coniacian transgression, likely
574 associated with subsidence caused by back-arc extension. Throughout the remainder of the
575 Cretaceous, the mixed-system exhibits weak progradation. A westerly topographic high formed by
576 a Lower Cretaceous submarine landslide complex deposited during earlier compression is

577 interpreted to have prevented deposition of the Cenomanian–Turonian toward the west. This
578 submarine landslide complex may also have provided a lateral source for landslides through
579 secondary remobilisation perpendicular to the regional palaeoflow from the north. Bed pinch-out,
580 thinning, ripple reflections and debrites provide further evidence for the presence of basinal
581 topography during deposition.

582

583 The Coniacian-Maastrichtian mixed siliciclastic-calcareous deep marine system contains both
584 siliciclastic and calcareous lobe elements, which represent different lobe sub-environments,
585 requiring modification of terminology developed for siliciclastic lobes. Mixed systems are also
586 shown to have unique facies, both in outcrop and a subsurface analogue from offshore The
587 Gambia, reflecting differing depositional processes between the systems operating
588 contemporaneously. Interaction between the two deep-marine environments characterising the
589 mixed systems has also made stacking patterns difficult to decipher, with each system attenuating
590 the other.

591

Acknowledgments

592 We are grateful to CASP for awarding a fieldwork grant for this project, to Chris Van Baak, Steve
593 Vincent, Rashad Gulmammadov for their logistical support and to Muslim Gazibayov for his
594 hospitality. Nigel Mountney is thanked for suggesting this study area in 2010. TGS are thanked
595 for permission to publish the seismic data

Facies	Description	Interpretation
Conglomerates (A)	0.1 to 3 + m thick beds of poorly-sorted, disorganised conglomerates. Most commonly clast-supported consisting of sub-angular to sub-rounded boulder-, cobble- and pebble-sized clasts of limestone and sandstone. Matrix comprises a poorly-sorted mix of all finer size fractions. Cm- 10cms scale mud-clasts occur sporadically throughout the beds. Bed bases are often erosive, and can be amalgamated. This facies often grades into thick bedded sandstones (C).	The characteristics of this facies suggest deposition from debris flows having cohesive as well as frictional strength (Fisher, 1971; Nemeck & Steel, 1984). The grading of conglomerates into thick-bedded sandstones reflects the transition of hyperconcentrated submarine debris flows into highly-concentrated turbulent flows (Mulder & Alexander, 2001; Sohn et al. 2002), due to the entrainment of ambient water (Postma et al. 1988).
Poorly sorted clast rich deposit (B)	0.1 – 1+ m thick poorly sorted deformed, matrix-supported units. Matrix can range from mudstone to coarse sandstone, and is often poorly-sorted and sheared. Clasts include cm-m scale limestone and sandstone blocks, rafts of remobilised folded thin-bedded sandstones, sporadic pebbles and granules and frequent mud-clasts. These deposits are commonly non-graded, but can show weak normal-grading.	The poorly-sorted matrix and large clast sizes are suggestive of ‘flow freezing’ of a flow with yield strength (Inverson et al. 2010), indicating ‘en masse’ deposition from a laminar flow (Nardin et al. 1979; Inverson 1997; Sohn 2000). Remobilised thin-bedded sandstones and intra-basinal clasts indicate localised mass failure and reworking.
Thick-bedded sandstones (C)	0.5 – 1+ m brown siliciclastic fine-granular sandstones. Normally-graded or non-graded and typically lacking in primary depositional structures. Bases are often sharp and erosive. Parallel laminations are sometimes present at bed tops and mud-clasts can be observed throughout. Weak cross-lamination is infrequently observed.	The general massive structuration of these deposits suggests that they represent rapid aggradation beneath a highly concentrated but dominantly turbulent flow, and are thus interpreted as high density turbidites (Lowe, 1982; Mutti 1992; Kneller & Branney 1995).
Mixed siliciclastic and calcareous sandstones (D)	0.1-1m beds of medium-bedded calcareous sandstones with punctuated interbeds of cm-scale thin-bedded siliciclastic sandstone, either as continuous beds or lenses. The medium-bedded calcareous sandstones are massive and the siliciclastic beds are often erosively-based and show tractional structures (ripple and planar lamination). Siliciclastic beds can be amalgamated with each other or isolated between calcareous siltstones or sandstones.	Medium-bedded calcareous sandstones are interpreted to represent deposition from a slowly aggrading dilute turbidity current. Periodic, thin-bedded siliciclastic sandstones represent deposition from a relatively quickly aggrading dilute turbidity current, which interacted with a much slower aggrading calcareous turbidity current.
Medium-bedded calcareous sandstones (E)	0.1-1 m thick beige beds of calcareous siltstone -fine sandstone. Normally-graded or non-graded. Planar lamination may be present, but other tractional structures are rare. Beds can be amalgamated.	Based on their tractional structures and normal-grading, beds are interpreted as having being deposited from dilute turbidity currents. These beds are interpreted as medium-density turbidites, due to larger bed thickness and infrequent tractional structures, than thin-bedded calcareous sandstones (G). Thicker beds and fine grain size indicate a slowly aggrading dilute turbidity current.
Medium-bedded siliciclastic sandstones (F)	0.1 -0.5 m thick brown beds of very fine – granular grained, commonly normally-graded, sandstones. Inverse-grading is infrequently observed. Basal parts of the bed are often structureless containing infrequent cm-scale mud-clasts while tops are rich in tractional structures including parallel, ripple and hummock-like laminations. Bed bases are often erosive, and can be amalgamated.	Based on their tractional structures and normal-grading, beds of this lithofacies are interpreted as deposition from a dilute turbidity current. These beds are interpreted as medium-density turbidites due to their bed thickness and common lack of structures in the lower part of the bed (e.g. Soutter et al. 2019).

Thin-bedded calcareous sandstones (G)	0.01 – 0.1 m thick beige beds of calcareous siltstone-fine sandstones. Can be normally-graded, often into silty-mudstones, or not graded. Planar laminations are observed but other tractional structures are typically absent. Individual beds are often amalgamated.	Thin-beds, fine grain size and weak planar laminations represent deposition from a low-concentration turbidity current (Mutti 1992; Jobe et al. 2012; Talling et al. 2012), indicating these beds are low-density turbidites. Fine grain size, thicker beds compared to thin-bedded siliciclastic sandstone (H) and absence of ripple laminations suggest slowly aggrading, dilute remnants of a turbulent flow, (Remacha & Fernández 2003; Bell et al. 2018), which did not reach significant velocity to generate ripple laminations (Baas et al. 2016).
Thin-bedded siliciclastic sandstones (H)	0.005 – 0.1 m thick brown beds of siliciclastic very fine- granular sandstones. Commonly normally-graded, occasional inverse-graded. Tractional structures (planar, ripple, hummock-like and convolute laminations) and sporadic mud-clasts are observed. Bases can be flat or weakly erosive and sometimes contain granules. Bed tops are often flat. Where present, ripples can show opposing palaeoflow.	Thin-bedded, structured sandstones are interpreted to be deposited from low-concentration turbidity currents (Mutti 1992; Jobe et al. 2012; Talling et al. 2012) and are therefore interpreted as low-density turbidites. Ripples with opposing palaeoflow suggests topographic interference.
Bi or tri-partite beds (I)	0.05-0.5 m thick beds that contain multiple parts. Typically consisting of a lower fine-coarse sandstone (division 1) overlain by a poorly-sorted muddy siltstone – medium sandstone (division 2). Division 3 is sometimes present consisting of a siltstone-fine grained sandstone loaded into division 2. Divisions 1 and 3 sometimes contain planar laminations and sporadic cm scale mud-clasts. Division 2 is often highly deformed and rich in mud-clasts and very coarse sandstone to pebble-grade clasts.	Tractional structures in division 1 and 3 indicate formation under turbulent flows. Poor-sorting and mud content suggest division 2 was deposited under a transitional-laminar flow regime. These bi-tri partite beds are hybrid beds (Haughton et al. 2009), generated by flow transformation from turbulent to laminar. Such transformation occurs through flow deceleration (Barker et al. 2008; Patacci et al. 2014) and by an increase in concentration of fines during flow run-out (Kane et al. 2017).
Mudstone (J)	0.005 – 8 m thick pale grey or red mudstone – fine siltstone beds, which are friable and often inferred in areas of missing section. Planar laminations, discontinuous drapes and lenses of siltstone may be present. Commonly calcareous in composition. Red beds are common at the base of the Campanian.	Low energy conditions, representative of background sedimentation via suspension fallout. Laminations may be present below the scale visible in outcrop, representing deposition from a dilute turbidity current (Boulestex et al. 2019). Pale colour indicates low total organic carbon (TOC). Red beds are similar to Cretaceous Oceanic Red Beds (CORBS) described across Europe (Wang et al. 2005; Hu et al. 2005; Wagneich & Krenmayr, 2005) and represent deposition below the carbonate compensation depth (CCD) in a deep oceanic basin.

References

- 598
599 AHMAD, R. & AFZAL, J. (2012) Sequence Stratigraphy of the Mixed Carbonate-Siliciclastic
600 System of the Eocene Nisai Formation, Pishin Basin. Distribution of Source Rocks and Reservoir
601 Facies.
602
- 603 AL-MASHAIKIE, S. & Mohammed, Y. (2017) Anatomy of carbonate breccias, turbidite facies
604 and depositional systems of Gercus Formation, in Donkan Area, Northern Iraq.
605
- 606 ALEXANDER, J. (2008) Bedforms in Froude-supercritical flow. Marine and River Dune
607 Dynamics.
608
- 609 ARAYA, T. & MASUDA, F. (2001) Sedimentary structures of antidunes: An overview. Journal of
610 the Sedimentological Society of Japan, 53, 1-15.
611
- 612 ARMITAGE, D.A., ROMANS, B.W., COVAULT, J.A. & GRAHAM, S.A. (2009) The influence
613 of mass-transport-deposit surface topography on the evolution of turbidite architecture: The Sierra
614 Contreras, Tres Pasos Formation (Cretaceous), southern Chile. Journal of Sedimentary
615 Research, 79(5), 287-301.
616
- 617 BAAS, J.H., BEST, J.L., PEAKALL, J. & WANG, M. (2009) A phase diagram for turbulent,
618 transitional and laminar clay suspension flows. Journal of Sedimentary Research, 79, 162-183.
619
- 620 BAAS, J., BEST, J. & PEAKALL, J. (2016) Predicting bedforms and primary current stratification
621 in cohesive mixtures of mud and sand. Journal of the Geological Society, 173(1), 12-45.
622
- 623 BARKER, S.P., HAUGHTON, P.D.W., MCCAFFREY, W.D., ARCHER, S.G. & HAKES, B.
624 (2008). Development of rheological heterogeneity in clay-rich high-density turbidity currents:
625 Aptian Britannia Sandstone Member, UK continental shelf. Journal of Sedimentary Research, 78,
626 45–68.
627
- 628 BASILICI, G., VIEIRA DE LUCA, P. H. & POIRÉ, D. G. (2012) Hummocky cross-
629 stratification-like structures and combined-flow reipples in the Punta Negra Formation (Lower-
630 Middle Devonian, Argentine Precordillera): A turbiditic deep-marine or storm-dominated prodelta
631 inner-shelf systems?. Sedimentary Geology, 267-268, 73-92.
632
- 633 BELL, D., STEVENSON, C.J., KANE, I.A., HODGSON, D.M. & POYATOS-MORÉ, M.
634 (2018) Topographic Controls On the Development of Contemporaneous but Contrasting Basin-
635 Floor Depositional Architectures. Journal of Sedimentary Research, 88(10), 1166-1189.
636
- 637 BELL, D., KANE, I., PONTÉN, A., FLINT, S., HODGSON, D. & BARRETT, B. (2018) Spatial
638 variability in depositional reservoir quality of deep-marine channel-fill and lobe deposits. Marine
639 and Petroleum Geology, 98, 97-115.
640

641 BLAIR, T.C. & MCPHERSON J.G. (1999) Grain-size and textural classification of coarse
642 sedimentary particles. *Journal of Sedimentary Research*, 69 (1), 6-19.

643

644 BOCHUD, M. (2011) *Tectonics of the Eastern Greater Caucasus in Azerbaijan* (Doctoral
645 Dissertation, University of Freiburg). p. 202.

646

647 BOULESTEIX, K., POYATOS-MORE, M., FLINT, S.S, TAYLOR, K.G., HODGSON, D.M.
648 AND HASIOTIS, S.T. (2019) Transport and Deposition of Mud in Deep-marine Environments:
649 Processes and Stratigraphic Implications. *Sedimentology*, 66 (7), 2894-2925.

650

651 BOUMA, A.H. (1962) *Sedimentology of some flysch deposits: a graphic approach to facies*
652 *interpretation*. Amsterdam, Elsevier, 168

653

654 BRAGA, J., MARTIN, J. & WOOD, J. (2001) Submarine lobes and feeder channels of
655 redeposited, temperate carbonate and mixed siliciclastic-carbonate platform deposits (Vera Basin,
656 Almeria, southern Spain). *Sedimentology* v. 48(1), 99-116.

657

658 BRAGINA, L. G. & BRAGIN, N.Y. (2015) New data on Albian-Coniacian radiolarians from
659 the Kelevudag section (northeastern Azerbaijan). *Stratigraphy and Geological Correlation*, 23 (1),
660 45-56.

661

662 BROOKS, H.L., HODGSON, D.M., BRUNT, R.L., PEAKALL, J. & FLINT, S.S. (2018)
663 Exhumed lateral margins and increasing flow confinement of a submarine landslide
664 complex. *Sedimentology*, 65(4), 1067-1096.

665

666 BRUNET M. F., KOROTAEV M.V., ERSHOV A.V. & NIKISHIN A.M. (2003) The South
667 Caspian Basin: a review of its evolution from subsidence modelling. *Sedimentary Geology*, 156 (1-
668 4), 119-148.

669

670 BULL, S., CARTWRIGHT, J. & HUUSE, M. 2009. A review of kinematic indicators from mass-
671 transport complexes using 3D seismic data. *Marine and Petroleum Geology*, 26(7), 1132-1151.

672

673 BURBANK, D.W., VERGÉS, J., MUNOZ, A. & BENTHAM, P. (1992) Coeval hindward- and
674 forward-imbricating thrusting in the south-central Pyrenees, Spain: Timing and rates of shortening
675 and deposition. *Geological Society of America Bulletin*, 104, 3-17.

676

677 CASSON, M.A., CALVÈS, G., REDFERN, J., HUUSE, M. & SAYERS, B. (2020) *in press*.
678 Cretaceous continental margin evolution from quantitative seismic geomorphology, offshore
679 NW Africa. *Basin Research*.

680

681 CHIARELLA, D., LONGHITANO, S.G. & TROPEANO, M. (2017). Types of mixing and
682 heterogeneities in siliciclastic-carbonate sediments. *Marine and Petroleum Geology*, 88, 617-627.

683

684 CREVELLO, P.D. & SCHLAGER, W. (1980). Carbonate debris sheets and turbidites, Exuma
685 Sound, Bahamas. *Journal of Sedimentary Research*, 50(4), 1121-1147.

686
687 CURRAY, J.R. & MOORE, D.G. (1971) Growth of the Bengal deep-sea fan and denudation in
688 the Himalayas. *Geological Society of America Bulletin*, 82(3), 563-572.
689
690 D'ARGENIO, B., FERRERI, V., RASPINI, A., AMODIO, S. & BUONOCUNTO, F. 1999.
691 Cyclostratigraphy of a carbonate platform as a tool for high-precision correlation. *Tectonophysics*,
692 315(1-4), 357-384.
693
694 DEPTUCK, M.E., SYLVESTER, Z., PIRMEZ, C. & O'BYRNE, C. (2007). Migration-
695 aggradation history and 3-D seismic geomorphology of submarine channels in the Pleistocene
696 Benin-major Canyon, western Niger Delta slope. *Marine and Petroleum Geology*, 24 (6-9), 406-
697 433.
698
699 DE BLASIO, F.V., ENGVIK, L.E. & ELVERHØI, A. (2006) Sliding of outrunner blocks from
700 submarine landslides. *Geophysical Research Letters*, 33(6).
701
702 DICKIE, J. & HEIN, F. (1995) Conglomeratic fan deltas and submarine fans of the Jurassic
703 Laberge Group, Whitehorse Trough, Yukon Territory, Canada: fore-arc sedimentation and
704 unroofing of a volcanic island arc complex. *Sedimentary Geology*, 98(1-4), 263-292.
705
706 DITTY, P.S., HARMON, C.J., PILKEY, O.H., BALL, M.M. & RICHARDSON, E.S. (1977)
707 Mixed terrigenous—Carbonate sedimentation in the Hispaniola—Caicos turbidite basin. *Marine*
708 *Geology*, 24(1), 1-20.
709
710 DORSEY, R.J. & KIDWELL, S.M. (1999) Mixed carbonate-siliciclastic sedimentation on a
711 tectonically active margin: Example from the Pliocene of Baja California Sur, Mexico. *Geology*,
712 27(10), 935-938.
713
714 DUNBAR, G.B. & DICKENS, G.R. (2003) Late Quaternary shedding of shallow-marine
715 carbonate along a tropical mixed siliciclastic–carbonate shelf: Great Barrier Reef,
716 Australia. *Sedimentology*, 50(6), 1061-1077.
717
718 EGAN, S.S., MOSAR, J., BRUNET, M.F. & KANGARLI, T. (2009) Subsidence and uplift
719 mechanisms within the South Caspian Basin: insights from the onshore and offshore Azerbaijan
720 region. *Geological Society, London, Special Publications*, 312(1), 219-240.
721
722 FALLGATTER, C., KNELLER, B., PAIM, P.S. & MILANA, J.P. (2017) Transformation,
723 partitioning and flow–deposit interactions during the run-out of megaflores:
724 *Sedimentology*, 64(2), 359-387.
725
726 FERGUSON, R.A., KANE, I.A., EGGENHUISEN, J.T., POHL, F., TILSTON, M.,
727 SPYCHALA, Y.T. & BRUNT, R.L. (2020) Entangled external and internal controls on submarine
728 fan evolution: an experimental perspective: *The Depositional Record*, in review.
729

730 FILDANI, A., CLARK, J., COVAULT, J.A., POWER, B., ROMANS, B. W. & AIELLO, I. W.
731 (2018) Muddy sand and sandy mud on the distal Mississippi fan: Implications for lobe depositional
732 processes: *Geosphere*, 14(3), 1051-1066.
733

734 FISHER, R.V. (1971) Features of coarse-grained, high concentration fluids and their deposits:
735 *Journal of Sedimentary Petrology*, 41, 916- 927.
736

737 FONNESU, M., FELLETTI, F., HAUGHTON, P.D., PATACCI, M. & MCCAFFREY, W.D.
738 (2018) Hybrid event bed character and distribution linked to turbidite system sub-environments:
739 The North Apennine Gottero Sandstone (north-west Italy). *Sedimentology*, 65(1), 151-190.
740

741 FRANCIS, J., DANIELL, J., DROXLER, A., DICKENS, G., BENTLEY, S., PETERSON, L.
742 BRADLEY, N. & BEAUFORT, L. (2008) Deep water geomorphology of the mixed siliciclastic-
743 carbonate system, Gulf of Papua: *Journal of Geophysical Research: Earth Surface*, 113(1).
744

745 GARCÍA-GARCÍA, F., SORIA, J., SAR VISERAS, C. & FERNÁNDEZ, J. (2009) High-
746 frequency rhythmicity in a mixed siliciclastic-carbonate shelf (Late Miocene, Guadix Basin, Spain):
747 A model of interplay between climatic oscillations, subsidence and sediment dispersal. *Journal of*
748 *Sedimentary Research*, 79, 302-315.
749

750 GAWTHORPE, R.L. (1986) Sedimentation during carbonate ramp-to-slope evolution in a
751 tectonically active area: Bowland Basin (Dinantian), northern England: *Sedimentology*, 33(2), 185-
752 206.
753

754 GEE, M.J.R., UY, H.S., WARREN, J., MORLEY, C.K. & LAMBIASE, J.J. (2007) The Brunei
755 slide: a giant submarine landslide on the North West Borneo Margin revealed by 3D seismic data.
756 *Marine Geology*, 246(1), 9-23.
757

758 GEORGIPOULOU, A., MASSON, D.G., WYNN, R.B. & KRASTEL, S. (2010) Sahara Slide:
759 Age, initiation, and processes of a giant submarine slide. *Geochemistry, Geophysics, Geosystems*,
760 11(7).
761

762 GOLDHAMMER, R.K., DUNN, P.A. & HARDIE, L.A. (1990) Depositional cycles, composite
763 sea level changes, cycle stacking patterns, and the hierarchy of stratigraphic forcing - examples
764 from platform carbonates of the Alpine Triassic. *Geological Society of America Bulletin*, 102, 535-
765 562.
766

767 GOLONKA, J. 2004. Plate tectonic evolution of the southern margin of Eurasia in the Mesozoic
768 and Cenozoic. *Tectonophysics*, 381(1-4), 235-273.
769

770 GRANT, R., UNDERHILL, J., HERNÁNDEZ-CASADO, J., BARKER, S. & JAMIESON, R.
771 (2019) Upper Permian Zechstein Supergroup carbonate-evaporite platform palaeomorphology in
772 the UK Southern North Sea. *Marine and Petroleum Geology*, 100, 484-518.
773

774 HAUGHTON, P.D.W., DAVIS, C., MCCAFFREY, W. & BARKER, S. (2009) Hybrid sediment
775 gravity flow deposits - Classification, origin and significance. *Marine and Petroleum Geology*, 26,
776 1900-1918.
777

778 HU, X., JANSÁ, L., WANG, C., SARTI, M., BAK, K., WAGREICH, M., MICHALIK, J. &
779 SOTAK, J. (2005) Upper Cretaceous oceanic red beds (CORBs) in the Tethys: occurrences,
780 lithofacies, age, and environments. *Cretaceous Research*, 26(1), 3-20.
781

782 HARMS, J., SOUTHARD, J., SPEARING, D., & WALKER, R. (1975). Depositional
783 Environments as Interpreted from Primary Sedimentary and Stratigraphic Sequences. SEPM.
784

785 HESSLER, A.M. & FILDANI, A. (2019) Deep-sea fans: tapping into Earth's changing
786 landscapes. *Journal of Sedimentary Research*, 89(11), 1171-1179.
787

788 HUBBARD, S.M., COVAULT, J.A., FILDANI, A. & ROMANS, B.W. (2014) Sediment transfer
789 and deposition in slope channels: Deciphering the record of enigmatic deep-sea processes from
790 outcrop. *Geological Society of America Bulletin*, 126, 857-871.
791

792 HUNTER, R.E. & CLIFTON, E.H. (1982) Cyclic deposits and hummocky cross-stratification of
793 probable storm origin in Upper Cretaceous rocks of the Cape Sebastian area, southwestern
794 Oregon. *Journal of Sedimentary Research*, 52(1), 127-143.
795

796 ILSTAD, T., DE BLASIO, F.V., ELVERHØI, A., HARBITZ, C.B., ENGVIK, L., LONGVA,
797 O. & MARR, J.G. (2004) On the frontal dynamics and morphology of submarine debris flows.
798 *Marine Geology*, 213(1-4), 481-497.
799

800 INVERSON, R.M. (1997) The physics of debris flows. *Reviews of Geophysics*, 35, 245-296.
801

802 INVERSON, R.M., LOGAN, M., LAHUSEN, R.G. & BERTI, M. (2010) The perfect debris
803 flow? Aggregated results from 28 largescale experiments. *Journal of Geophysical Research: Earth*
804 *Surface*, 115, 1-29.
805

806 JACKSON, C.A-L. (2011) Three-dimensional seismic analysis of megaclast deformation within a
807 mass transport deposit; implications for debris flow kinematics. *Geology*, 39(3), 203-206.
808

809 JOBE, Z.R., LOWE, D.R. & MORRIS, W.R. (2012) Climbing-ripple successions in turbidite
810 systems: depositional environments, sedimentation and accumulation times. *Sedimentology*, 59,
811 867-898.
812

813 JOBE, Z.R., SYLVESTER, Z., HOWES, N., PIRMEZ, C., PARKER, A., CANTELLI, A.,
814 SMITH, R., WOLINKSKY, M.A., O'BRYNE, C., SLOWEY, N. & PRATHER, B. (2017) High-
815 resolution, millennial-scale patterns of bed compensation on a sand-rich intraslope submarine fan,
816 western Niger Delta slope. *GSA Bulletin*, 129, 23-37.
817

818 JOHNSON, A.M. (1970) *Physical Processes in Geology*. San Francisco: Freeman, Cooper and
819 Company.
820

821 KANE, I.A. & HODGSON, D.M. (2011) Sedimentological criteria to differentiate submarine
822 channel levee subenvironments: Exhumed examples from the Rosario Fm. (Upper Cretaceous) of
823 Baja California, Mexico, and the Fort Brown Fm. (Permian), Karoo Basin, S. Africa. *Marine and*
824 *Petroleum Geology*, 28, 807-823.
825

826 KANE, I.A., PONTÉN, A.S., VANGDAL, B., EGGENHUISEN, J.T., HODGSON, D.M. &
827 SPYCHALA, Y.T. (2017) The stratigraphic record and processes of turbidity current
828 transformation across deep-marine lobes. *Sedimentology*, 64(5), 1236-1273.
829

830 KANE, I.A. & PONTÉN, A.S.M. (2012) Submarine transitional flow deposits in the Paleogene
831 Gulf of Mexico. *Geology*, 40, 1119–1122.
832

833 KANE, I.A., MCCAFFREY, W.D. & MARTINSEN, O.J. (2009) Allogenic vs. Autogenic
834 Controls on Megafault Formation. *Journal of Sedimentary Research*, v. 9, 643-651.
835

836 KANE, I.A., DYKSTRA, M.L., KNELLER, B.C., TREMBLAY, S. & MCCAFFREY, W.D.
837 (2009) Architecture of coarse-grained channel-levée system: the Rosario Formation, Baja
838 California, Mexico. *Sedimentology*, 56 (7), 2207-2234.
839

840 KILHAMS, B., HARTLEY, A., HUUSE, M. & DAVIS, C. (2012) Characterizing the Paleocene
841 turbidites of the North Sea: The Mey Sandstone Member, Lista Formation, UK Central Graben.
842 *Petroleum Geoscience*, 18(3), 337-354.
843

844 KILHAMS, B., HARTLEY, A., HUUSE, M. & DAVIS, C. (2015) Characterizing the Paleocene
845 turbidites of the North Sea: Maureen formation, UK Central Graben. *Geological Society Special*
846 *Publication*, 403, 43-62.
847

848 KNAUST, D., WARCHOL, M. & KANE, I.A. (2014) Ichnodiversity and ichnoabundance:
849 revealing depositional trends in a confined turbidite system. *Sedimentology*, 61 (7), 2218-2267.
850

851 KNELLER, B. C. & BRANNEY, M.J. (1995) Sustained high-density turbidity currents and the
852 deposition of thick massive sands. *Sedimentology*, 42, 607-616.
853

854 KNELLER, B., EDWARDS, D., MCCAFFREY, W. & MOORE, R. (1991) Oblique reflection of
855 turbidity currents. *Geology*, 19(3), 250-252.
856

857 KNELLER, B., BOZETTI, G., CALLOW, R., DYKSTRA, M., HANSEN, L., KANE, I., LI, P.,
858 MCARTHUR, A., CATHARINA, A.S., SANTOS, T.D. & THOMPSON, P (2020) Architecture,
859 process, and environmental diversity in a late Cretaceous slope channel system. *Journal of*
860 *Sedimentary Research*, 90, 1-26.
861

862 KOPAEVICH, L.F., BENIAMOVSKII, V.N. & BRAGINA, L.G. (2015) Upper Albian-Turonian
863 foraminifers and radiolarians from the Kelevudag section, northeastern Azerbaijan. *Stratigraphy
864 and Geological Correlation*, 23(6), 580-599.
865

866 LI, P., KNELLER, B.C., THOMPSON, P., BOZETTI, G. & DOS SANTOS, T. (2018)
867 Architectural and facies organisation of slope channel fills: Upper Cretaceous Rosario Formation,
868 Baja California, Mexico. *Marine and Petroleum Geology*, 92, 632–649.
869

870 LOWE, D.R. (1982) Sediment gravity flows: Depositional models with special reference to the
871 deposits of high-density turbidity currents. *Journal of Sedimentary Research*, 52, 279-297.
872

873 MARINI, M., MILLI, S., RAVNAS, R. & MOSCATELLI, M. (2015) A comparative study of
874 confined vs. semi-confined turbidite lobes from the Lower Messinian Laga Basin (Central
875 Apennines, Italy): implications for assessment of reservoir architecture. *Marine and Petroleum
876 Geology*, 63, 142–165.
877

878 MCARTHUR, A., KANE, I., BOZETTI, G., HANSEN, L. & KNELLER, B. (2019) Supercritical
879 flows overspilling from bypass-dominated submarine channels and the development of overbank
880 bedforms: The Depositional Record.
881

882 MCHARGUE, T. R., HODGSON, D. M. & SHELEF, E. (2019) Architectural Diversity of
883 Submarine Lobes. *EarthArXiv*.
884

885 MILLER, R.P. & HELLER, P.L. (1994) Depositional framework and controls on mixed
886 carbonate-siliciclastic gravity flows: Pennsylvanian-Permian shelf to basin transect, south-western
887 Great Basin, USA. *Sedimentology*, 41(1), 1-20.
888

889 MILLER, K.G., SUGARMAN, P.J., BROWNING, J.V., KOMINZ, M.A., HERNÁNDEZ, J.C.,
890 OLSSON, R.K., WRIGHT, J.D., FEIGENSON, M.D. & VAN SICKEL, W. (2003) Late
891 Cretaceous chronology of large, rapid sea-level changes: Glacioeustasy during the greenhouse
892 world. *Geology*, 31(7), 585-588.
893

894 MITCHELL, S.F., PICKERILL, R.K. & STEMANN, T.A. (2001) The Port Morant Formation
895 (Upper Pleistocene, Jamaica): high resolution sedimentology and paleoenvironmental analysis of a
896 mixed carbonate clastic lagoonal succession. *Sedimentary Geology*, 144(3-4), 291-306.
897

898 MOSCARDELLI, L., OCHOA, J., LUNT, I. & ZAHM, L. (2019) Mixed siliciclastic–carbonate
899 systems and their impact for the development of deep-marine turbidites in continental margins: A
900 case study from the Late Jurassic to Early Cretaceous Shelburne subbasin in offshore Nova
901 Scotia. *AAPG Bulletin*, 103(10), 2487-2520.
902

903 MOUNT, J.F. (1984) Mixing of siliciclastic and carbonate sediments in shallow shelf
904 environments. *Geology*, 12, 432-435.
905

906 MULDER, T. & ALEXANDER, J. (2001) Abrupt change in slope causes variation in the
907 deposit thickness of concentrated particle-driven density currents. *Marine Geology*, 175(1-4),
908 221-235.
909

910 MULDER, T., ZARAGOSI, S., RAZIN, P., GRELAUD, C., LANFUMEY, V. & BAVOIL, F.
911 (2009) A new conceptual model for the deposition process of homogenite: Application to a
912 cretaceous megaturbidite of the western Pyrenees (Basque region, SW France). *Sedimentary
913 Geology*, 222(3-4), 263-273.
914

915 MUELLER, P., PATACCI, M. & DI GIULIO, A. (2017) Hybrid event beds in the proximal to
916 distal extensive lobe domain of the coarse-grained and sand-rich Bordighera turbidite system
917 (NW Italy). *Marine and Petroleum Geology*, 86, 908-931.
918

919 MUTTI, E. (1977) Distinctive thin-bedded turbidite facies and related depositional environments
920 in the Eocene Hecho Group (South-central Pyrenees, Spain). *Sedimentology*, 24, 107–131.
921

922 MUTTI, E. (1983) The Hecho Eocene submarine fan system, south-central Pyrenees,
923 Spain. *GeoMarine Letters*, 3(2-4), 199-202.
924

925 MUTTI, E. (1992) Turbidite sandstones: AGIP- Istituto di Geologia, Università di Parma, p. 275.
926

927 NARDIN, T.R., HEIN, F.J., GORSLINE, D.S. & EDWARDS, B.D. (1979) A review of mass
928 movement processes, sediment and acoustic characteristics, and contrasts in slope and base-of-
929 slope systems versus canyon-fan-basin floor systems. *SEPM Special Publications*, 27, 61-73.
930

931 NEMEC, W. & STEEL, R.J. (1984) Alluvial and Coastal Conglomerates: Their Significant
932 Features and Some Comments on Gravelly Mass-Flow Deposits.
933

934 NIKISHIN, A.M., CLOETINGH, S., BRUNET, M-F., STEPHENSON, R.A., BOLOTOV, S.N.
935 & ERSHOV, A.V. (1998). Scythian Platform, Caucasus and Black Sea region: Mesozoic-Cenozoic
936 tectonic history and dynamics. In: *Peri-Tethys Memoir 3: stratigraphy and evolution of Peri-
937 Tethyan platforms* (Ed. by Crasquin-Soleau, S. and Barrier, É.) *Mémoires du Muséum national
938 d'Histoire naturelle*, Paris, 177, 163-176.
939

940 NIKISHIN A.M., ZIEGLER P., PANOV, D.I., NAZAREVICH B.P., BRUNET M., F.,
941 STEPHENSON R.A., BOLOTOV S.N., KORATAEV M.V. & TIKHOMROV P.L. (2001)
942 Mesozoic and Cainozoic evolution of the Scythian Platform - Black Sea - Caucasus domain. In:
943 *Peri-Tethys Memoir 6 - Peri-Tethyan rift/wrench basins and passive margins* (Ed. by Ziegler P.,
944 Cavazza W., Robertson A.H.F. & Crasquin-Soleau S.), *Mémoires du Muséum national d'Histoire
945 naturelle*, Paris, 186, 295-346.
946

947 NISSEN, S.E., HASKELL, N.L., STEINER, C.T. & COTERILL, K.L. (1999) Debris flow
948 outrunner blocks, glide tracks, and pressure ridges identified on the Nigerian continental slope
949 using 3-D seismic coherency. *The Leading Edge*, 18(5), 595-599.
950

- 951 NORMARK, W.R., PIPER, D.J.W. & HESS, G.R. (1979) Distributary channels, sand lobes, and
 952 mesotopography of Navy submarine fan, California Borderland, with applications to ancient fan
 953 sediments. *Sedimentology*, 26(6), 749-774.
 954
- 955 PATACCI, M., HAUGHTON, P.D. & MCCAFFREY, W.D. (2014) Rheological complexity in
 956 sediment gravity flows forced to decelerate against a confining slope, Braux, SE France. *Journal*
 957 *of Sedimentary Research*, 84, 270-277.
 958
- 959 PEAKALL, J., MCCAFFREY, B. & KNELLER, B. (2000) A process model for the evolution,
 960 morphology, and architecture of sinuous submarine channels: *Journal of Sedimentary Research*,
 961 70, 434-448.
 962
- 963 PICKERING, K.T. & CORREGIDOR, J. (2005) Mass-transport complexes (MTCs) and tectonic
 964 control on basin-floor submarine fans, middle Eocene, south Spanish Pyrenees. *Journal of*
 965 *Sedimentary Research*, 75(5), 761-783.
 966
- 967 POPRAWSKI, Y., BASILE, C., AGIRREZABALA, L., JAILLARD, E., GAUDIN, M. &
 968 JACQUIN, T. (2014) Sedimentary and structural record of the Albian growth of the Bakio salt
 969 diapir (the Basque Country, northern Spain). *Basin Research*, 26(6), 746-766.
 970
- 971 POPRAWSKI, Y., BASILE, C., JAILLARD, E., GAUDIN, M., AND LOPEZ, M. (2016)
 972 Halokinetic sequences in carbonate systems: An example from the Middle Albian Bakio Breccias
 973 Formation (Basque Country, Spain). *Sedimentary Geology*, 334, 34-52.
 974
- 975 POSTMA, G. (1984) Mass-flow conglomerates in a submarine canyon: Abrioja fan-delta, Pliocene,
 976 southeast Spain. In: *Sedimentology of Gravels and Conglomerates*, Canadian Society of Petroleum
 977 Geologists Memoir (Ed. by Koster, E.H. & Steel, R.J.), 10, 237-258.
 978
- 979 POSTMA, G. (1984) Slumps and their deposits in fan delta front and slope (sedimentation model,
 980 Spain). *Geology*, 12(1), 27-30.
 981
- 982 POSTMA, G., NEMEC, W. & KLEINSPEHN, K. (1988) Large floating clasts in turbidites: a
 983 mechanism for their emplacement. *Sedimentary Geology*, 58 (1), 47-61.
 984
- 985 POSTMA, G., HILGEN, F.J. & ZACHARIASSE, W.J. (1993) Precession-punctuated growth of
 986 a late Miocene submarine-fan lobe on Gavdos (Greece). *Terra nova*, 5(5), 438-444.
 987
- 988 PRÉLAT, A., HODGSON, D.M. & FLINT, S.S. (2009) Evolution, architecture and hierarchy of
 989 distributary deep-water deposits: a high-resolution outcrop investigation from the Permian Karoo
 990 Basin, South Africa. *Sedimentology*, 56(7), 2132-2154.
 991
- 992 PRÉLAT, A. & HODGSON, D.M. (2013) The full range of turbidite bed thickness patterns in
 993 Submarine lobes: Controls and implications. *Journal of the Geological Society*, v. 170(1), pp. 209-
 994 214.
 995
- 996 PUGA-BERNABÉU, Á., WEBSTER, J., BEAMAN, R., REIMER, P. & RENEMA, W. (2014)

- 997 Filling the gap: A 60ky record of mixed carbonate-siliciclastic turbidite deposition from the Great
998 Barrier Reef. *Marine and Petroleum Geology*, 50, 40-50.
999
- 1000 REMACHA, E. & FERNÁNDEZ, L.P. (2003) High-resolution correlation patterns in the
1001 turbidite systems of the Hecho Group (South-Central Pyrenees, Spain). *Marine and Petroleum*
1002 *Geology*, 20, 711–726.
1003
- 1004 ORTIZ-KARPF, A., HODGSON, D.M. & MCCAFFREY, W.D. (2015) The role of mass-
1005 transport complexes in controlling channel avulsion and the subsequent sediment dispersal
1006 patterns on an active margin: the Magdalena Fan, offshore Colombia. *Marine and Petroleum*
1007 *Geology*, 64, 58-75.
1008
- 1009 OSLEGER, D.A. & MONTAÑEZ, I.P. (1996) Cross-platform architecture of a sequence
1010 boundary in mixed siliciclastic-carbonate lithofacies, Middle Cambrian, southern Great Basin,
1011 USA. *Sedimentology*, 43(2), 197-217.
1012
- 1013 SAINTOT, A., STEPHENSON, R.A., STOVBA, S., BRUNET, M.F., YEGOROVA, T. &
1014 STAROSTENKO, V. (2006) The evolution of the southern margin of Eastern Europe (Eastern
1015 European and Scythian platforms) from the latest Precambrian-Early Palaeozoic to the Early
1016 Cretaceous: *Geological Society, London, Memoirs*, 32(1), 481-505.
1017
- 1018 SALLER, A.H., BARTON, J.W. & BARTON, R.E. (1989) Slope sedimentation associated with a
1019 vertically building shelf, Bone Spring Formation, Mescalero Escarpe field, southeastern New
1020 Mexico. In: *Controls on carbonate platform and basin development* (Ed. by P.D. Crevello, J.J.
1021 Wilson, J.F. Sarg, and J.F. Read), *Society of Economic Paleontologists and Mineralogists*, pp. 275-
1022 288.
1023
- 1024 SCOTT, E., GELIN, F., JOLLEY, S., LEENAARTS, E., SADLER, S. & ELSINGER, R. (2010)
1025 Sedimentological control of fluid flow in deep marine turbidite reservoirs: Pierce Field, UK Central
1026 North Sea. *Geological Society Special Publication*, 347, 113-132.
1027
- 1028 SOBIESIAK, M.S., KNELLER, B., ALSOP, G.I. & MILANA, J.P. (2016) Inclusion of substrate
1029 blocks within a mass transport deposit: a case study from Cerro Bola, Argentina. In: *Submarine*
1030 *Mass Movements and Their Consequences*, pp. 487-496. Springer.
1031
- 1032 SOHN, Y.K. (2000) Depositional processes of submarine debris flows in the Miocene fan deltas,
1033 Pohang Basin, SE Korea with special reference to flow transformation. *Journal of Sedimentary*
1034 *Research*, 70, 491–503.
1035
- 1036 SOHN, Y., CHOE, M. & JO, H. (2002) Transition from debris flow to hyperconcentrated
1037 flow in a submarine channel (the Cretaceous Cerro Toro formation, southern Chile). *Terra*
1038 *Nova*, 14(5), 405-415.
1039

1040 SOSSON, M., STEPHENSON, R., SHEREMET, Y., ROLLAND, Y., ADAMIA, S.,
1041 MELKONIAN, R., KANGARLI, T., YEGOROVA, T., AVAGYAN, A., GALOYAN, G. &
1042 DANELIAN, T. (2016) The eastern Black Sea-Caucasus region during the Cretaceous: New
1043 evidence to constrain its tectonic evolution. *Comptes Rendus Geoscience*, 348(1), 23-32.
1044

1045 SOUTTER, E.L., KANE, I.A. & HUUSE, M. (2018) Giant submarine landslide triggered by
1046 Paleocene mantle plume activity in the North Atlantic. *geology*, 46(6), 511-514.
1047

1048 SOUTTER, E.L., KANE, I.A., FUHRMANN, A., CUMBERPATCH, Z.A. & HUUSE, M. (2019)
1049 The Stratigraphic Evolution of Onlap in Clastic Deep-marine Systems: Autogenic Modulation of
1050 Allogenic Signals. *Journal of Sedimentary Research*, 89 (10), 890-917.
1051

1052 SPYCHALA, Y.T., HODGSON, D.M., PRÉLAT, A., KANE, I.A., FLINT, S.S. &
1053 MOUNTNEY, N.P. (2017) Frontal and lateral submarine lobe fringes: comparing sedimentary
1054 facies, architecture and flow processes. *Journal of Sedimentary Research*, 87, 75-96.
1055

1056 STEVENSON, C.J., JACKSON, C.A-L., HODGSON, D.M., HUBBARD, S.M. &
1057 EGGENHEISEN, J.T. (2015) Deep-marine sediment bypass: *Journal of Sedimentary Research*,
1058 85, 1058-1081.
1059

1060 STOW, D.A.V. & MAYALL, M. (2000) Deep-marine sedimentary systems: new models for the
1061 21st
1062 Century. *Marine and Petroleum Geology*, 17, 125-135
1063

1064 STRAUB, K., PAOLA, C., MOHRIG, D., WOLINSKY, M. & GEORGE, T. (2009)
1065 Compensational stacking of channelized sedimentary deposits. *Journal of Sedimentary Research*,
1066 79, 673-688.
1067

1068 SURLYK, F. (1984) Fan-delta to submarine fan conglomerates of the Volgian-Valanginian
1069 Wollaston Forland Group, East Greenland. In: *Sedimentology of Gravels and Conglomerates*:
1070 Canadian Soc. of Petroleum Geologists, Memoir (Ed. by E. H. Koster & R. J. Steel), 10, 359-382.
1071

1072 SUMNER, E.J., PEAKALL, J., PARSONS, D.R., WYNN, R.B., DARBY, S.E., DORRELL,
1073 R.M., MCPHAIL, S.D., PERRETT, J., WEBB, A. & WHITE, D. (2013) First direct measurements
1074 of hydraulic jumps in an active submarine density current. *Geophysical Research Letters*, 40, 5904-
1075 5908.
1076

1077 SYLVESTER, Z. & LOWE, D.R. (2004) Textural trends in turbidites and slurry beds from the
1078 Oligocene flysch of the East Carpathians, Romania. *Sedimentology*, 51, 945-972.
1079

1080 TALLING, P., MASSON, D. SUMNER, E. & MALGESINI, G. (2012) Subaqueous sediment
1081 density flows: Depositional processes and deposit types. *Sedimentology*, 59, 1937-2003.
1082

- 1083 TASSY, A., CROUZY, E., GORINI, C., RUBINO, J.L., BOUROULLEC, J.L. & SAPIN, F.
1084 (2015) Egyptian Tethyan margin in the Mesozoic: Evolution of a mixed carbonate-siliciclastic shelf
1085 edge (from Western Desert to Sinai). *Marine and Petroleum Geology*, 68, 565-581.
1086
- 1087 TERLAKY, V., ROCHELEAU, J. & ARNOTT, R.W.C. (2016) Stratal composition and
1088 stratigraphic organization of stratal elements in an ancient deep-marine basin-floor succession,
1089 Neoproterozoic Windermere Supergroup, British Columbia, Canada. *Sedimentology*, 63(1), 136-
1090 175
1091
- 1092 TINTERRI, R., LAPORTA, M. & OGATA, K. (2017) Asymmetrical cross-current turbidite facies
1093 tract in a structurally-confined mini-basin (Priabonian–Rupelian, Ranzano Sandstone, northern
1094 Apennines, Italy). *Sedimentary Geology*, 352, 63–87.
1095
- 1096 TUCKER, M.E. (2003) Mixed clastic–carbonate cycles and sequences: Quaternary of Egypt and
1097 Carboniferous of England. *Geologia Croatica*, 56(1), 19-37.
1098
- 1099 VAN WAGONER J.C., MITCHUM R.M., CAMPION K.M. & RAHMANIAN V.D. (1990)
1100 Siliciclastic Sequence Stratigraphy in Well Logs, Cores, and Outcrop: Concepts for High-
1101 Resolution Correlation of Facies. American Association of Petroleum Geologists Methods in
1102 Exploration Series, pp. 55.
1103
- 1104 VINCENT, S.J., MORTON, A.C., CARTER, A., GIBBS, S. & BARABADZE, T.G. (2007)
1105 Oligocene uplift of the Western Greater Caucasus: an effect of initial Arabia–Eurasia
1106 collision. *Terra Nova*, 19(2), 160-166.
1107
- 1108 WAGREICH, M. & KRENMAYR, H. (2005) Upper Cretaceous oceanic red beds (CORB) in the
1109 Northern Calcareous Alps (Nierental Formation, Austria): Slope topography and clastic input as
1110 primary controlling factors. *Cretaceous Research*, 26(1), 57-64.
1111
- 1112 WALKER, R.G. (1978) Deep-marine sandstone facies and ancient submarine fans: Models for
1113 exploration for stratigraphic traps. *AAPG Bulletin*, 62, 932-966.
1114
- 1115 WALKER, W., JOBE, Z. R., WOOD, L. & SARG, R. (2019) Progradational Slope Architecture
1116 and Sediment Partitioning in the Outcropping Mixed Siliciclastic-Carbonate Bone Spring
1117 Formation, Permian Basin, west Texas. *EarthArXiv*
1118
- 1119 WANG, C., HU, X., SARTI, M., SCOTT, R. & LI, X. (2005) Upper Cretaceous oceanic red beds
1120 in southern Tibet: A major change from anoxic to oxic, deep-sea environments. *Cretaceous*
1121 *Research*, 26(1), 21-32.
1122
- 1123 WESCOTT, W.A. & ETHRIDGE, F.G. (1983). Eocene fan delta-submarine fan deposition in
1124 the Wagwater Trough, east-central Jamaica. *Sedimentology*, 30(2), 235-247.
1125

1126 YOSE, L.A. & HELLER, P.L. (1989) Sea-level control of mixed-carbonate-siliciclastic, gravity-
1127 flow deposition: Lower part of the Keeler Canyon Formation (Pennsylvanian), southeastern
1128 California. *Geological Society of America Bulletin*, 101(3), 427-439.

1129

1130 ZELLER, M., VERWER, K., EBERLI, G.P., MASSAFERRO, J.L., SCHWARZ, E. &
1131 SPALLETTI, L. (2015) Depositional controls on mixed carbonate–siliciclastic cycles and
1132 sequences on gently inclined shelf profiles. *Sedimentology*, 62(7), 2009-2037.

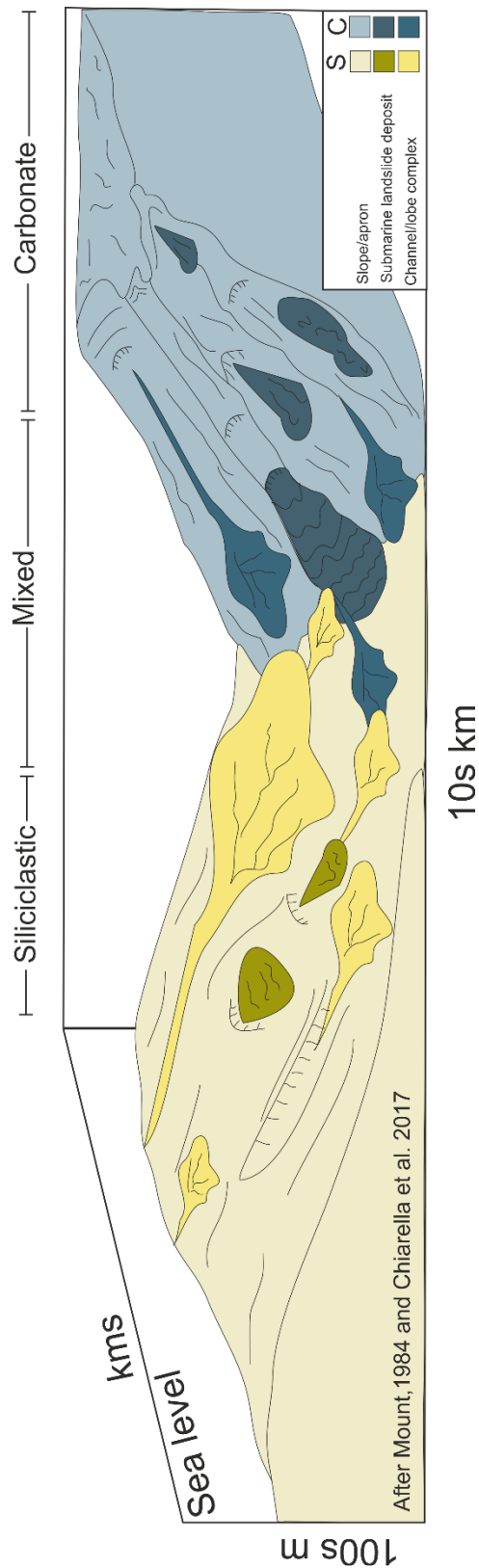
1133

1134 ZONNEVELD, J.P., MOSLOW, T.F. & HENDERSON, C.M. (1997) Lithofacies associations
1135 and depositional environments in a mixed siliciclastic-carbonate coastal depositional system, upper
1136 Liard Formation, Triassic, northeastern British Columbia. *Bulletin of Canadian Petroleum
1137 Geology*, 45(4), 553-575.

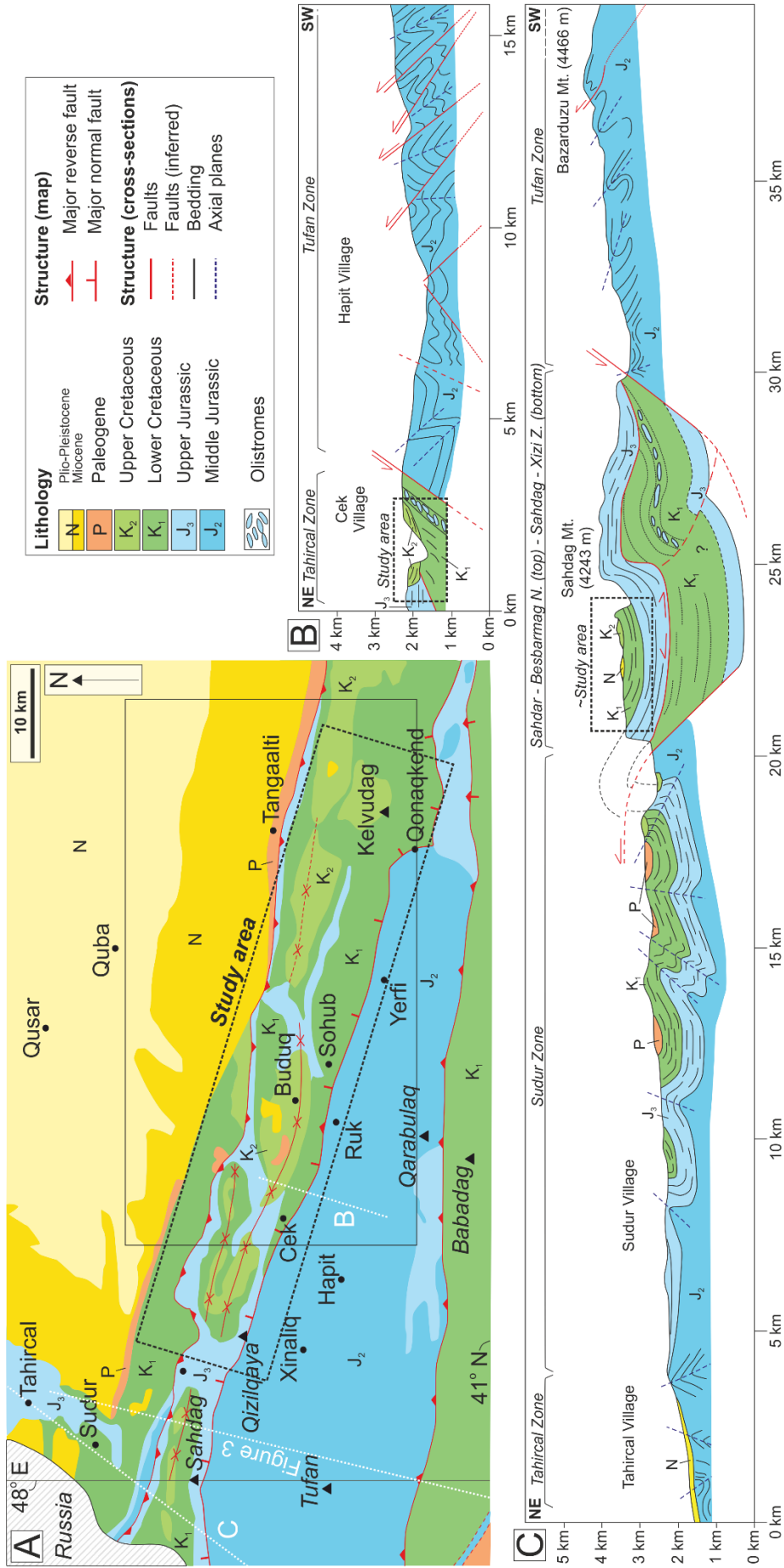
1138

1139 **FIGURES**

1140

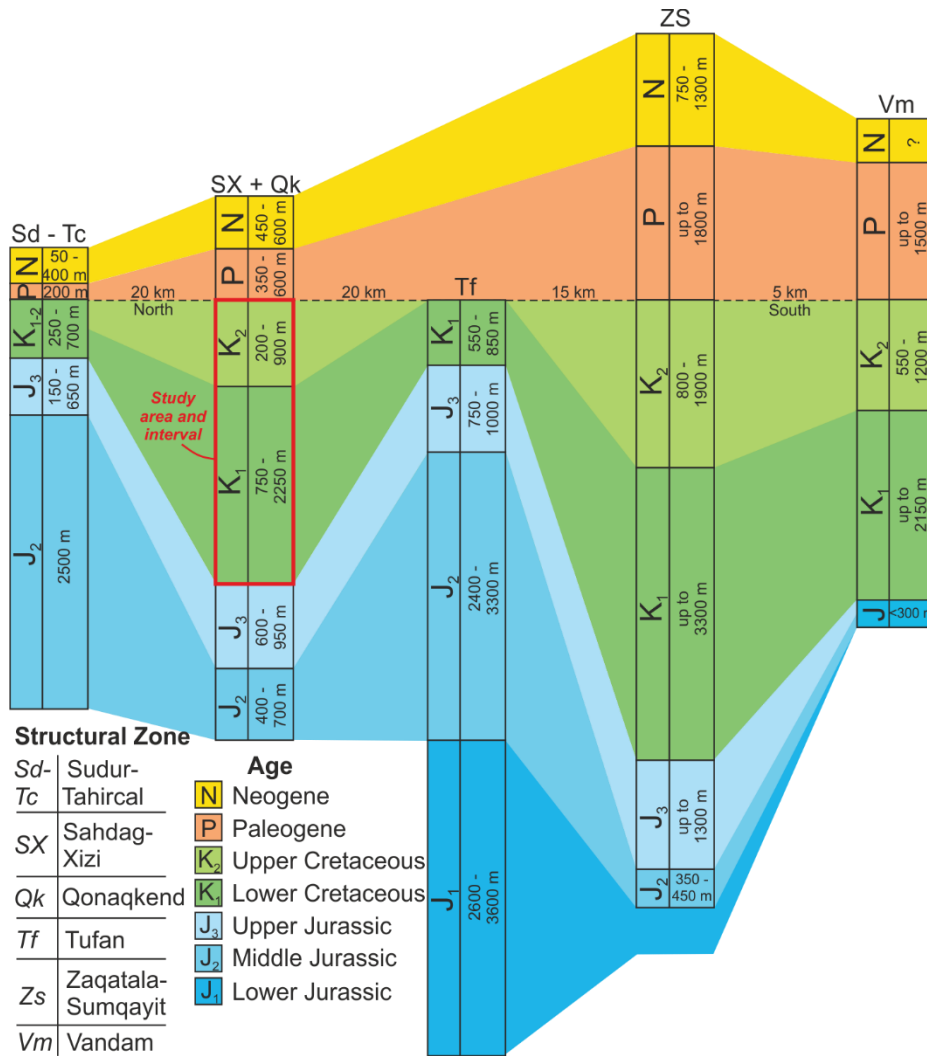


1141
 1142 Figure 1: Simplified conceptual model showing how siliciclastic and carbonate systems may
 1143 interact at a basin-scale in a deep-marine mixed siliciclastic-carbonate system. Carbonate material
 1144 is shed from a shallower carbonate-producing platform that periodically received siliciclastic
 1145 material; this is then redeposited in the deep-marine by of gravity flows (After Mount 1984,
 1146 Chiarella et al. 2017).
 1147



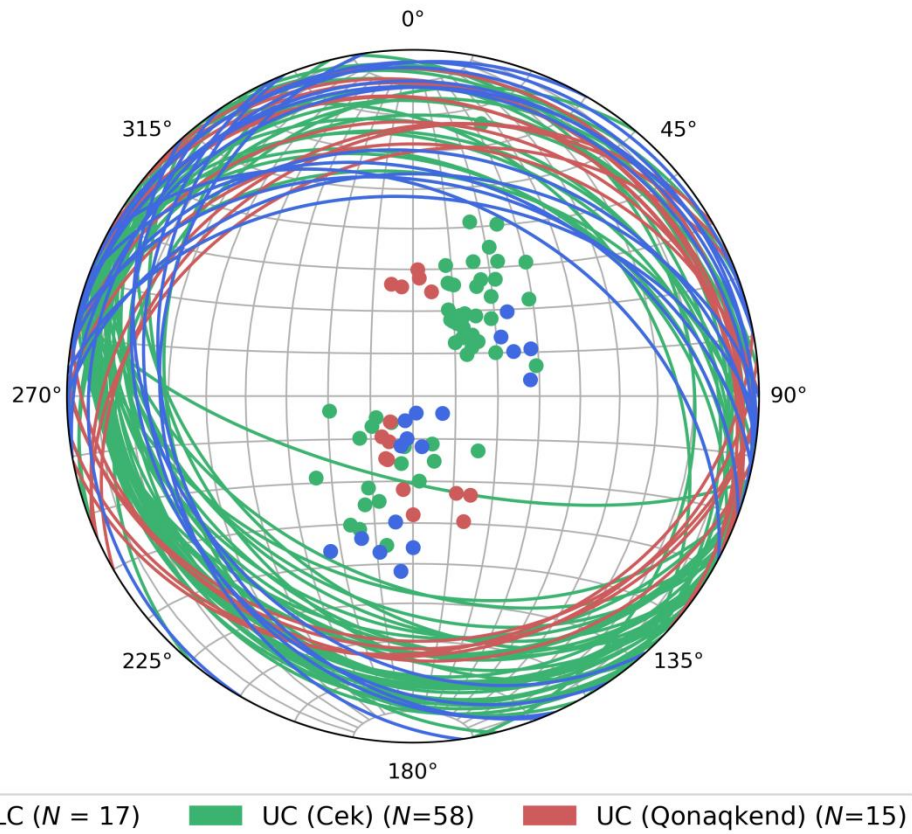
Lithology		Structure (map)	
Yellow	Plio-Pleistocene	Red triangle	Major reverse fault
Orange	Miocene	Red line with perpendicular ticks	Major normal fault
Green	Paleogene	Red dashed line	Faults
Light Green	Upper Cretaceous	Red dashed line with perpendicular ticks	Faults (inferred)
Dark Green	Lower Cretaceous	Red dashed line with perpendicular ticks	Bedding
Light Blue	Upper Jurassic	Black dashed line	Axial planes
Dark Blue	Middle Jurassic	Black dashed line	
Blue with wavy lines	Olistromes		

1149 Figure 2: Structural and stratigraphic framework of the Eastern Greater Caucasus (EGC) of
 1150 Azerbaijan. A) Simplified geological map, black box locates study area, lines B and C are located.
 1151 Schematic location of Figure 3 is shown. B) Cross section across the Cek-Hapit Valley, black box
 1152 locates study area. C) Cross section from Tahircal-Sahdag Mountain – Bazarduzu Mountain,
 1153 black box locates equivalent stratigraphy to our studied section (Modified from Bochud, 2011).
 1154
 1155
 1156
 1157
 1158



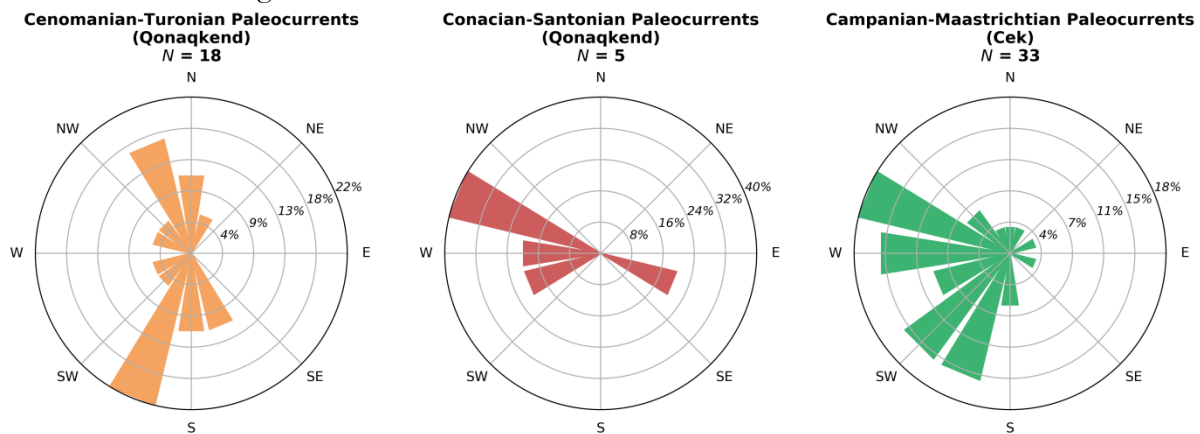
1159 Figure 3: Stratigraphic section trending roughly north-south across the five main structural zones
 1160 (from Bochud 2011) of the EGC. Flattened along the top of the Cretaceous, located on Figure 2.
 1161

Cretaceous Structure of the Qonaqkend Zone



1162
1163
1164
1165
1166
1167

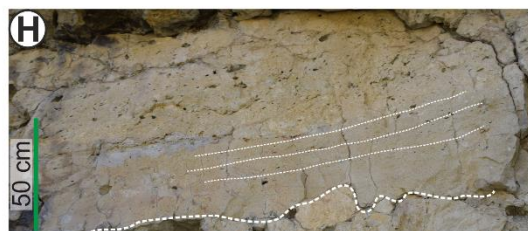
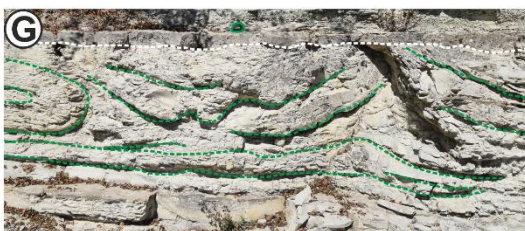
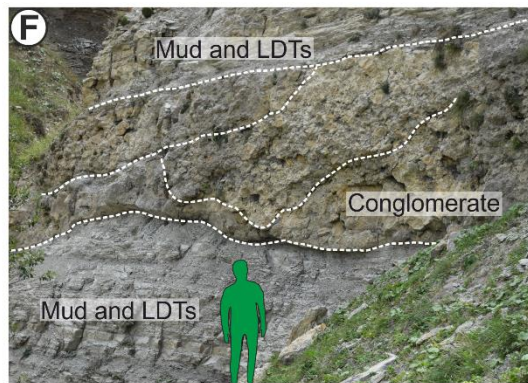
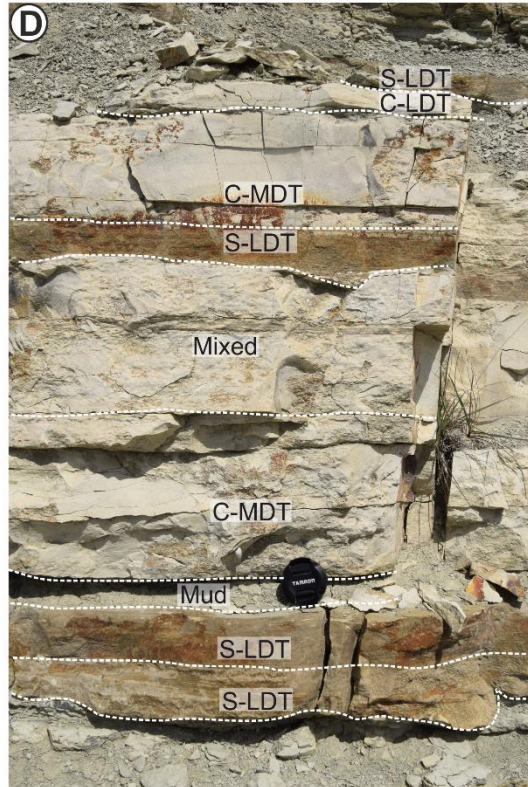
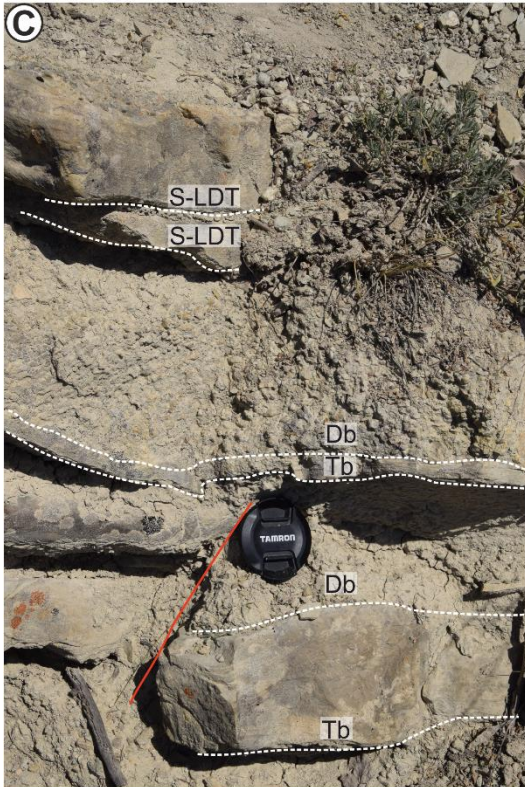
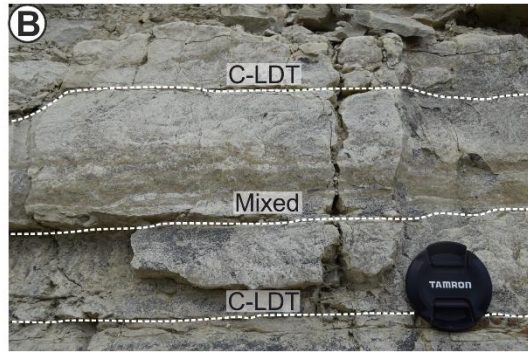
Figure 4: Equal area stereographic projection showing bedding readings for Cretaceous stratigraphy across Qonaqkend Zone. Bedding planes shown as lines and poles to bedding shown as dots. Coloured by stratigraphy and location; LC- Lower Cretaceous, UC- Upper Cretaceous. Structural data reveals a shallow-moderate structural dip to the north and south, in agreement with the east-west trending structural zones of the EGC.



1168
1169
1170
1171

Figure 5: Rose diagrams from palaeocurrent indicators (ripples, sole marks, cross-stratification) from the Cretaceous stratigraphy of the Qonaqkend Zone. Readings have been corrected for tectonic tilt and are subdivided by stratigraphy and location (see Figure 2).

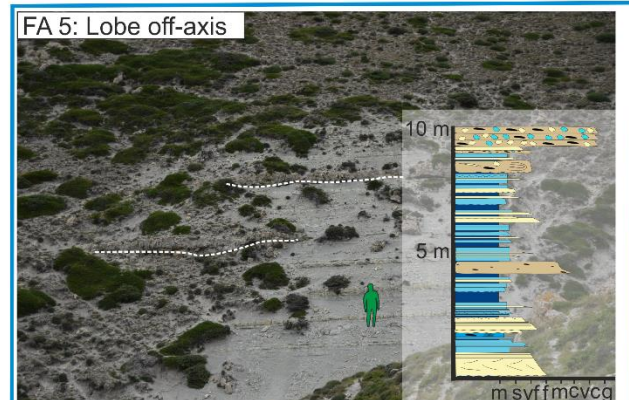
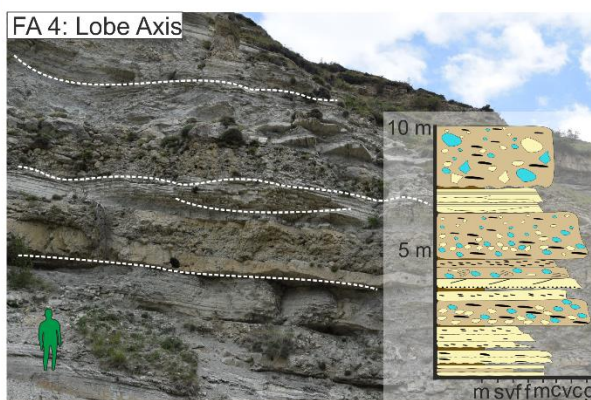
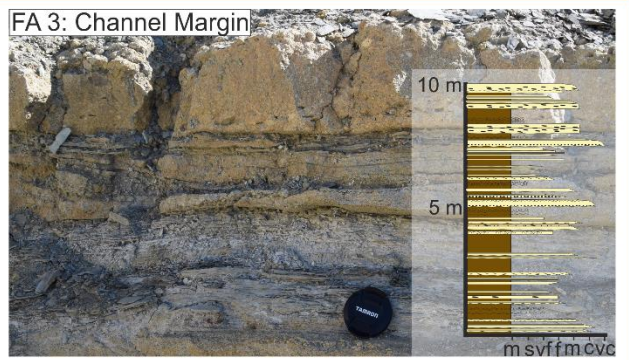
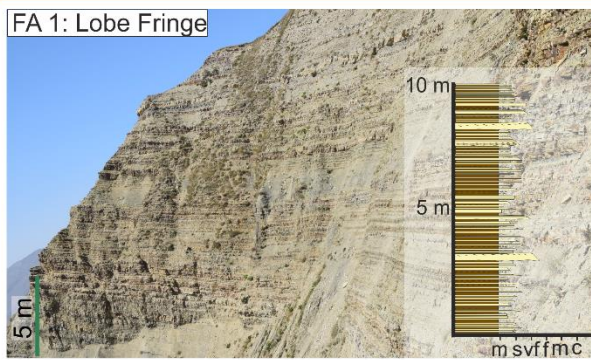
1172
1173



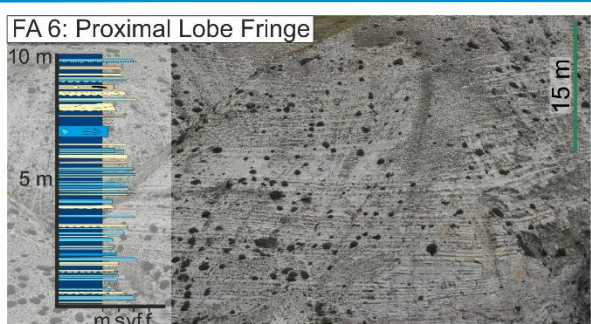
1175 Figure 6: Facies photographs. Facies described in detail in Table 1. Scale is either lens cap (52
1176 mm), person (1.74 m) or indicated. LDT; low density turbidite, MDT; medium density turbidite,
1177 Db; debrite (poorly sorted clast rich deposit); Tb; Turbidite, S; Siliciclastic, C; Calcareous. A)
1178 Calcareous mudstone B) Calcareous low density turbidite and mixed beds (of siliciclastic and
1179 calcareous low density turbidites). C) Two bi-partite beds consisting of a lower turbidite and an
1180 upper debrite, in this case both siliciclastic, overlain by two siliciclastic low density turbidites. D)
1181 Evidence for facies scale mixing (sensu Chiarella et al. 2017); calcareous turbidites were
1182 recognised in the field by their pale cream colour, while siliciclastic turbidites were brown-orange
1183 in colour and contained visual quartz granules. Calcareous turbidite probably accumulated slowly
1184 based on their grain size, and were punctuated by siliciclastic gravity flows, forming mixed beds.
1185 E) Siliciclastic low and medium density turbidites with cm-scale mud clasts weathered out. F)
1186 Mudstone and low density turbidites (both calcareous and siliciclastic) punctuated by metre-scale
1187 amalgamated conglomerates. G) Chaotic, clast rich-deposit with deformed, non-extensive
1188 bedding. Camera lens cap circled in green. H) Erosionally-based, crudely cross-laminated
1189 siliciclastic high density turbidite rich in mud clasts.

1190

Siliciclastic Facies Associations



Mixed Facies Associations



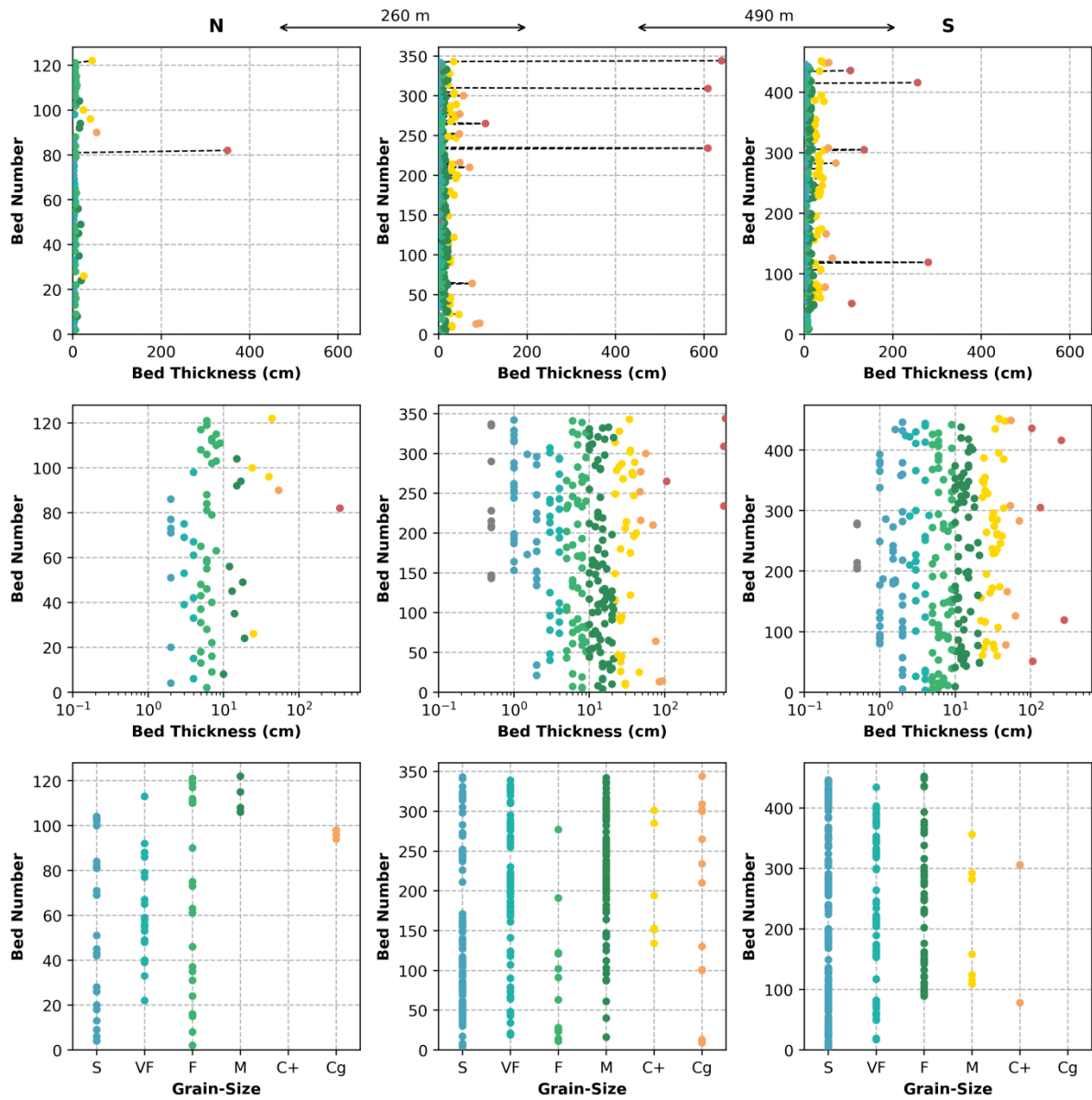
Key to all logs

Siliciclastic turbidite	Siliciclastic debris	Siliciclastic mudstone	Calci-turbidite	Calci-debrite	Clasts (coloured by lithology)
Planar lamination	Ripple lamination	Cross bedding	Granular horizon	Convolute lamination	Wavy bedding
Erosional contact	Slump	Mud clasts	Amalgamation	Sporadic pebble	Beds <2 cm thick

1191
1192
1193
1194
1195

Figure 7: Type examples of the seven recognised facies associations, divided into siliciclastic and mixed (siliciclastic and calcareous) associations, by orange and blue boxes respectively. Scale either lens cap (52 mm), person (1.74 m) or indicated. 10 m type log is taken from representative logged section of each facies association. Cretaceous Oceanic Red Beds; CORBS.

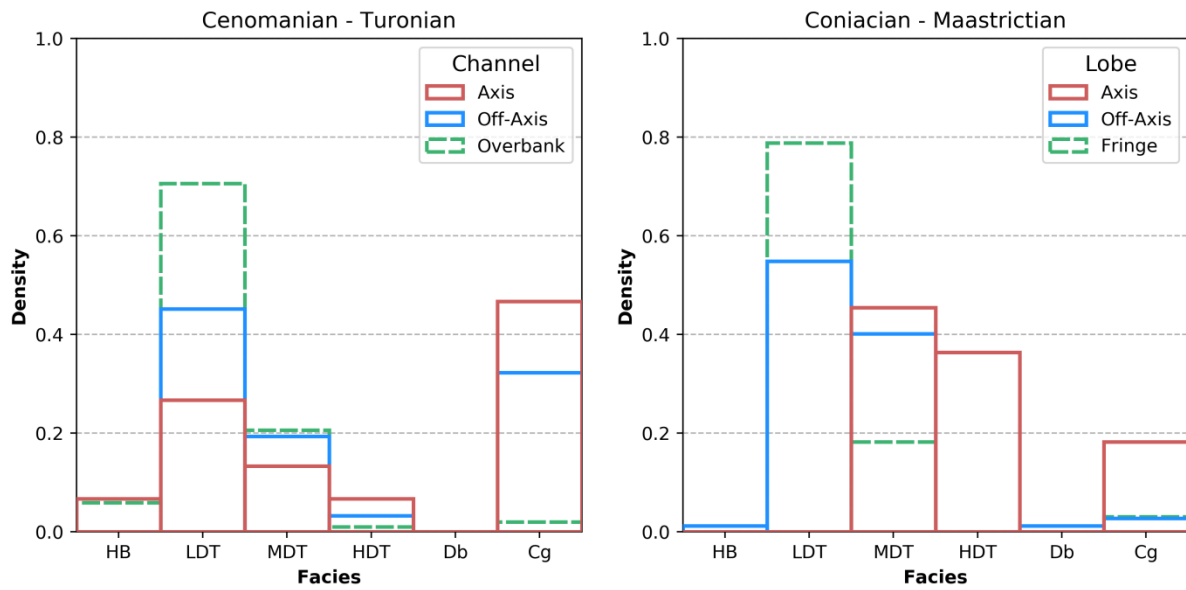
Coniacian-Maastrichtian Bed Statistics



1196
1197
1198
1199
1200
1201
1202
1203
1204
1205

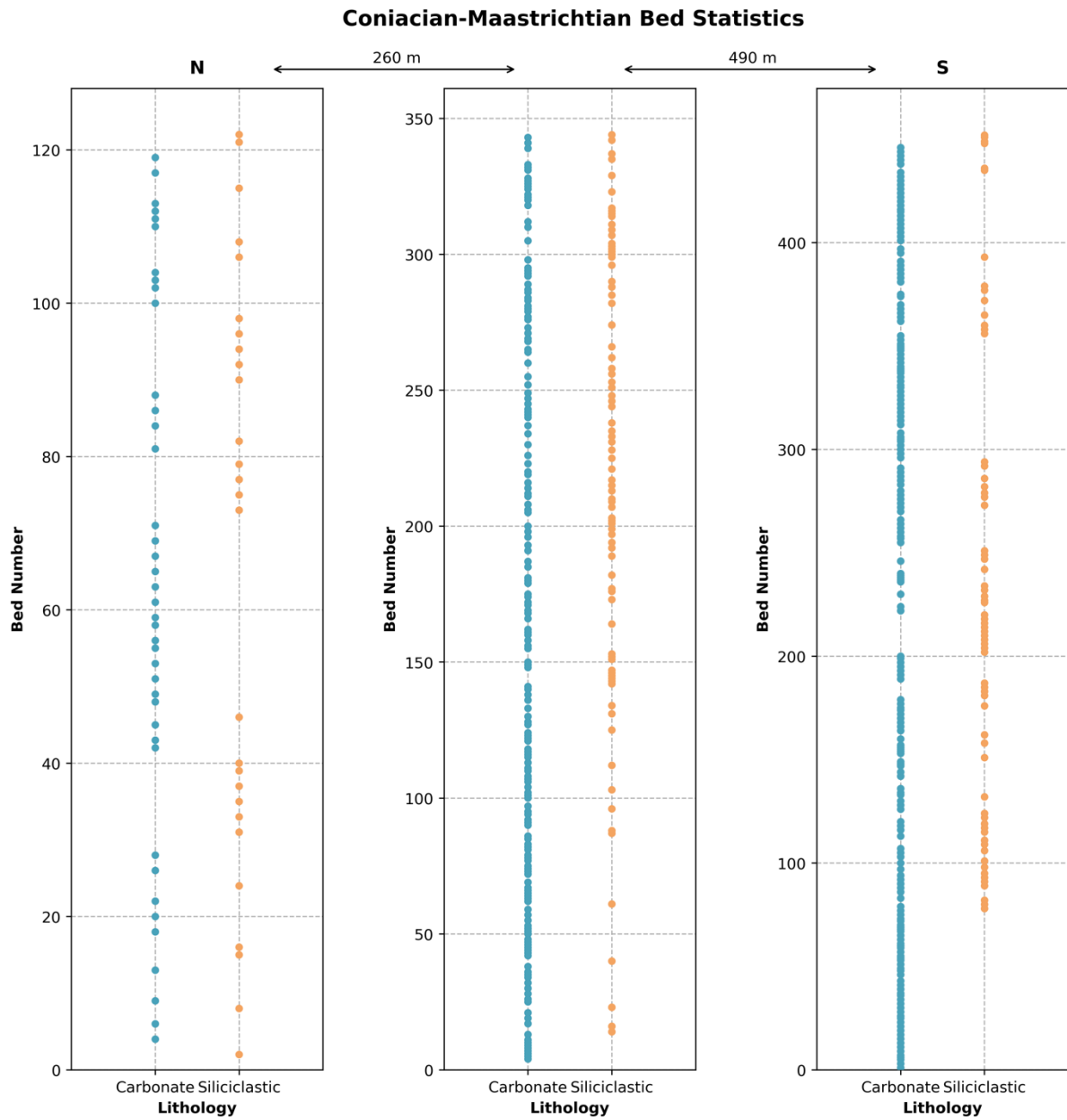
Figure 8: Quantitative facies analysis for Coniacian-Maastrichtian stratigraphy. The three columns represent three different logged sections from north to south that are representative of northern margin, axis and southern margin of the basin respectively. Charts compare bed number (with 1 being at the base of the log and 200 at the top) to bed thickness (linearly in the top column and logarithmically in the middle column) and logged grain size (in the basal column). Where grain size varies within the bed average grain size is used. In the top column thick beds are highlighted with a dashed line. Colours are for visual separation of data, and meaning changes per column, blue are thin/fine beds/grain-size, oranges are thick/coarse beds/grain-sizes. Scales for bed number vary across the rows.

Upper Cretaceous Facies Associations



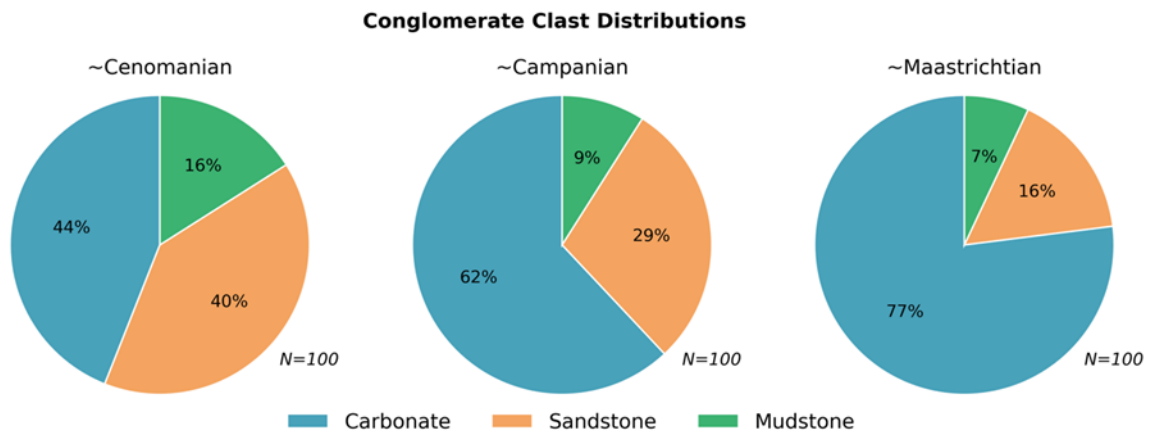
1206
1207
1208
1209
1210
1211
1212

Figure 9: Quantative facies analysis for Upper Cretaceous stratigraphy, divided into Cenomanian-Turonian channelised siliciclastic deposition and Coniacian – Maastrichtian mixed lobe deposition. Facies refer to HB: hybrid bed (bi and tri-partite beds); LDT: low density turbidite; MDT: medium density turbidite; HDT: high density turbidite; Db: debrite (poorly sorted clast rich deposit) and Cg: conglomerate. Coloured by type log for different sub-environment. Density refers to the percentage of each facies in each log.



1213
1214
1215
1216

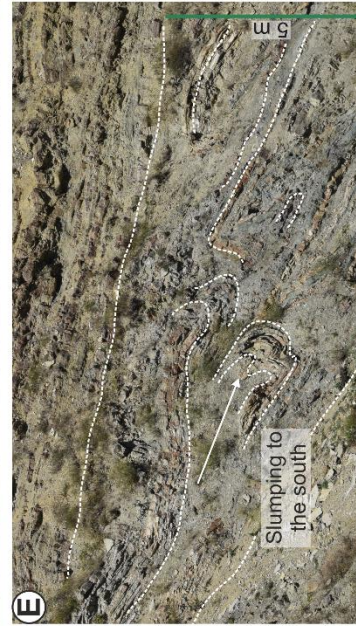
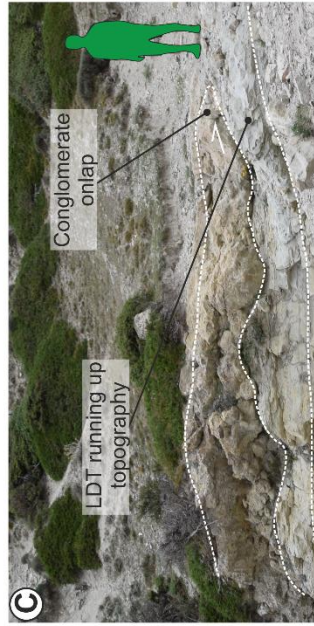
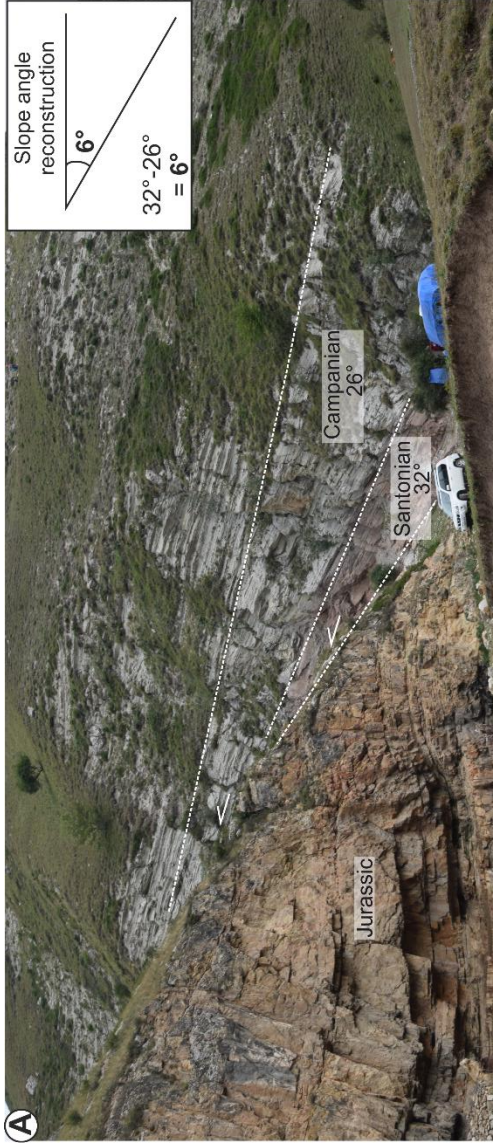
Figure 10: Quantitative facies analysis of Coniacian-Maastrichtian mixed stratigraphy comparing bed composition (carbonate or siliciclastic) against bed number (height up log). Using the same logged sections as Figure 8, and thus a different number of beds per log resulting in variable bed number scale.



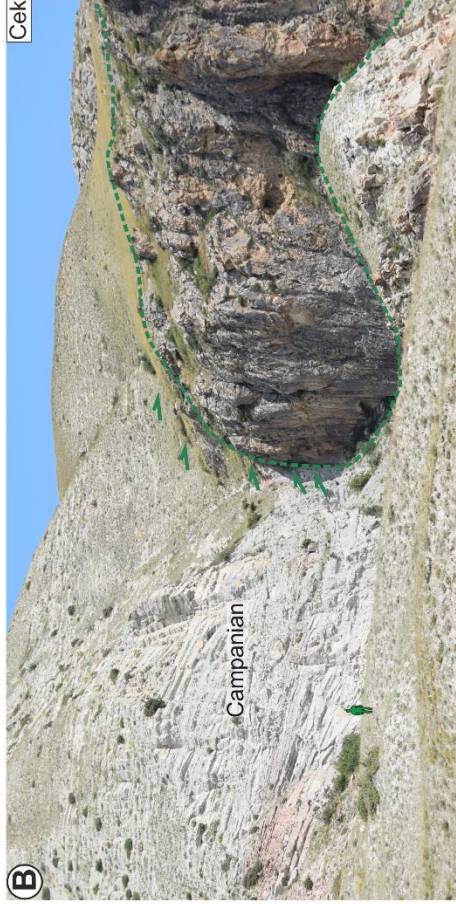
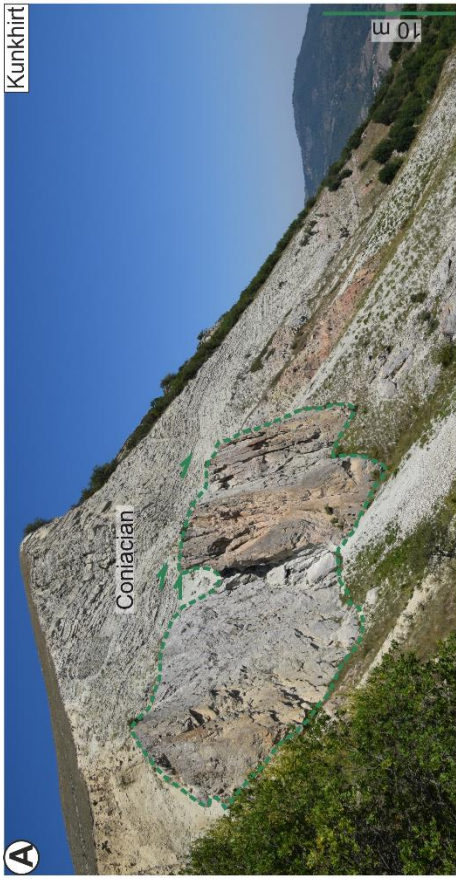
1217

1218 Figure 11: Pie charts showing composition of clasts within conglomerates per stratigraphic age, taken
1219 from 100 clasts from representative conglomeratic beds of over 1 metre thick. Percentage equates to
1220 absolute number of clasts, as 100 are sampled. Carbonate clast content increases through time, discussed
1221 in text.

1222

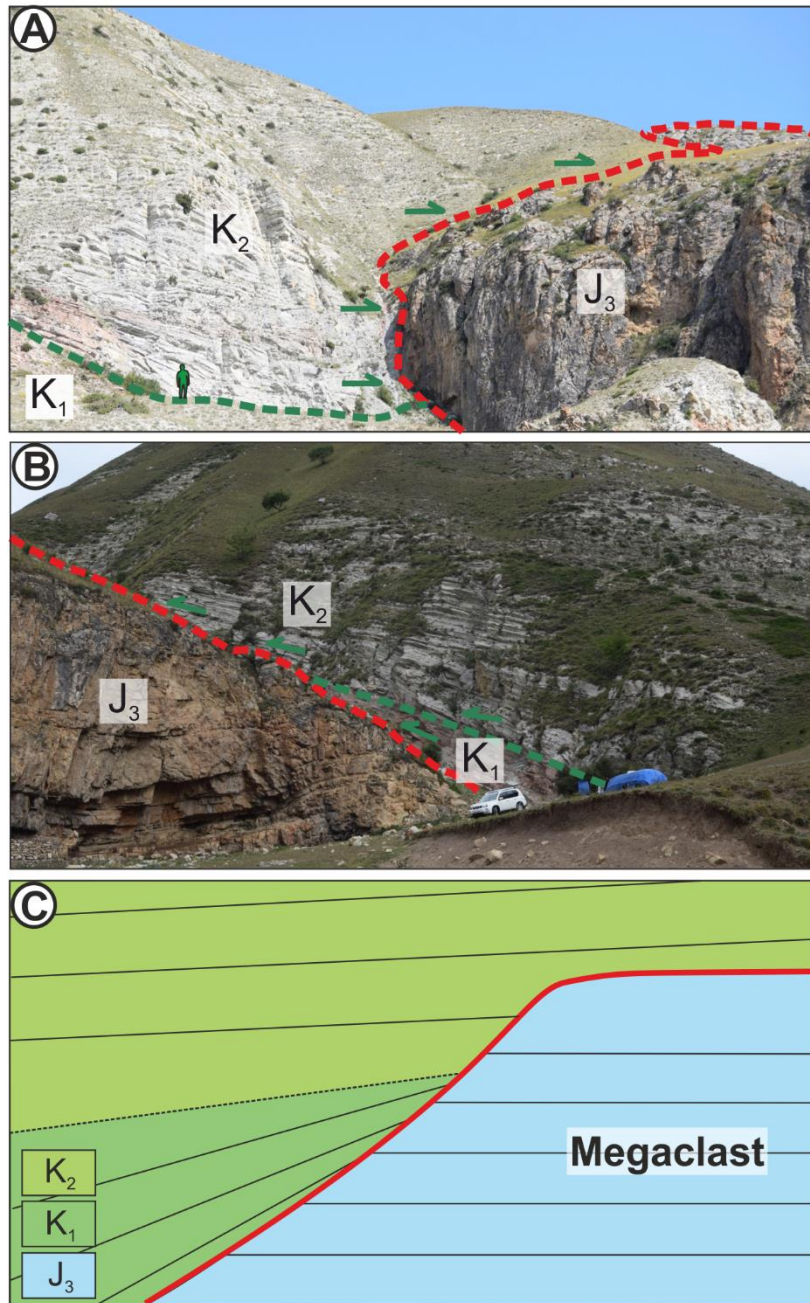


1224 Figure 12: Evidence for palaeotopography. Scale indicated by person (1.74m), car (1.9 m) or
1225 indicated. A) Cretaceous stratigraphy thinning and onlapping Jurassic limestone, slope angle
1226 reconstructed. B) Evidence for opposing ripple directions suggesting flow reflection. C)
1227 Thickness and pinch-out variability of different deposits on a metre-scale laterally. D) Cliff
1228 section containing three conglomerate bodies which vary in architecture and termination style as
1229 indicated. E) Submarine landslide deposit showing evidence for slumping towards the south.

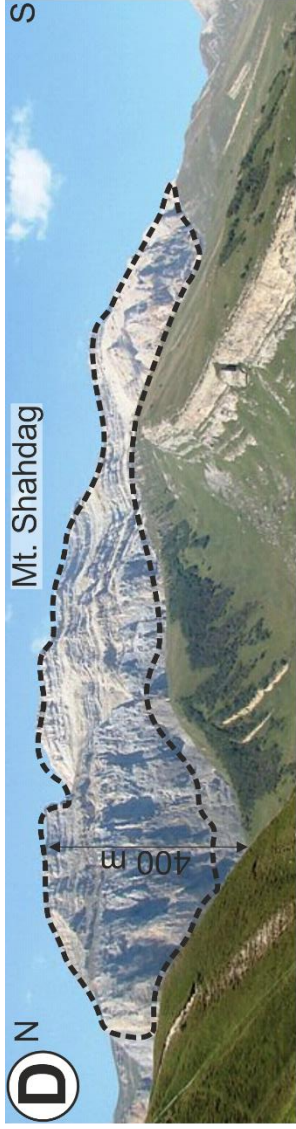


1231 Figure 13: Evidence for collapse of the Jurassic carbonate platform. Scale is shown by person (1.74 m),
 1232 car (1.9 m) or indicated. Onlap indicated by green arrows, extent of clast or bedding surface shown in
 1233 green dashed line. A) Metre-scale limestone clasts within Coniacian mixed stratigraphy at Kunkhirt. B)
 1234 Campanian calcareous low density turbidites abutting against a decametre-scale Jurassic limestone block
 1235 at Cek. C) Stacked, inversely-graded submarine landslide deposits primarily composed of reworked
 1236 Jurassic limestone blocks at Rük, upwards widening triangles indicate coarsening upwards (inverse-
 1237 grading). D) In situ break-up of the Jurassic platform at Cek. Clasts are fractured and separated but
 1238 bedding planes (indicated in white) are still visible showing minimal displacement.

Jurassic - Cretaceous contact



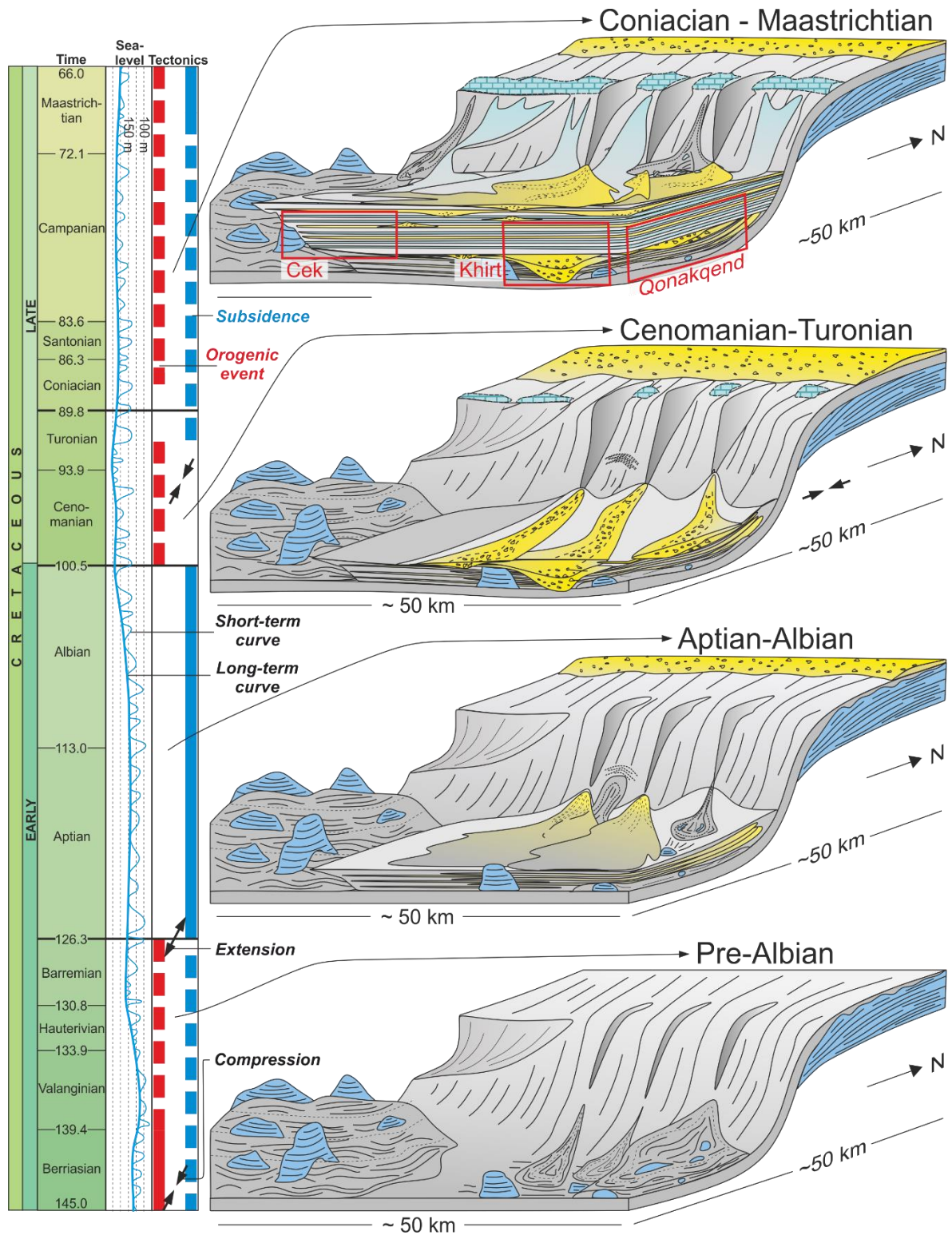
1239 Figure 14: Evidence and model for the generation of topography by an allochthonous block throughout
 1240 the Cretaceous. A&B) field examples of Jurassic stratigraphy forming topography throughout the
 1241 Cretaceous influencing sediment routing. C) Schematic model showing formation of topography.
 1242



1244 Figure 15: Evidence for allochthonous block model as the most likely for the generation of
1245 Cretaceous topography. Scale is shown by person (1.74 m) or indicated. Blocks are drawn
1246 around with black dashed line. A-C are examples of metre-decametre scale clasts around Cek. D)
1247 Shahdag Mountain, the tallest mountain in Azerbaijan, is interpreted as a kilometre-scale wide
1248 olistostrome by Bochud, 2011. E) Block with both margins exposed and overlapped by mixed
1249 stratigraphy, black box locates C.

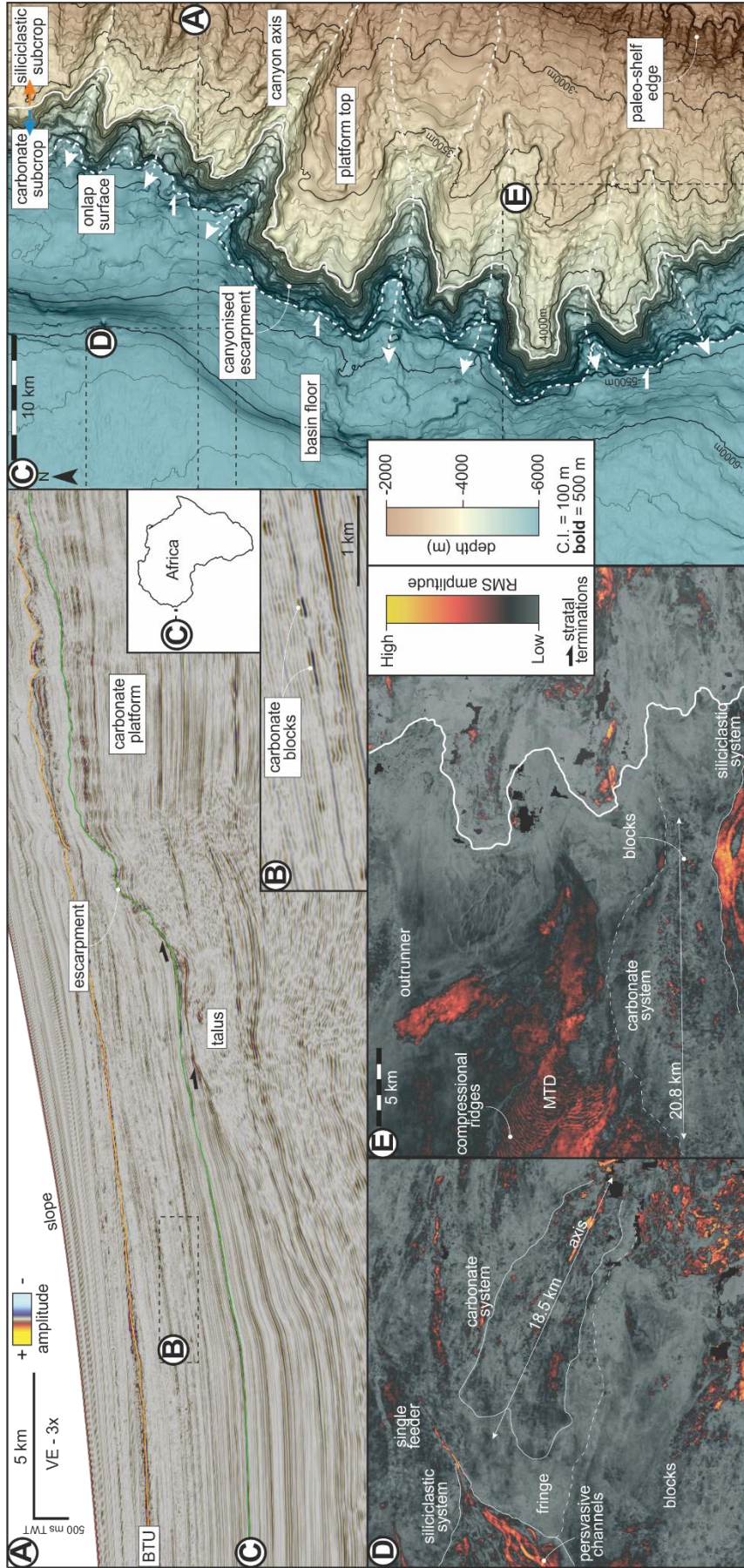
1250

1251



1252
 1253
 1254
 1255
 1256
 1257
 1258
 1259
 1260

Figure 16: Evolutionary model for the Cretaceous of the study area. Studied stratigraphic sections highlighted. Topography, thought to be formed by a mega-clast, is present throughout the Cretaceous and influences deposition, discussed in text. Extract from the geological time column, sea level fluctuations and local tectonic events highlighted on the left. The Pre-Albian was dominated by limestone blocks on a muddy slope. Thin-bedded siliciclastics of a distal lobe were deposited during the Aptian-Albian. Siliciclastic channels are prominent throughout the Cenomanian-Turonian. In the Coniacian-Maastrichtian mixed calcareous and siliciclastic lobes, of different sub-environments interact, and are likely sourced from the same northern margin.



1262 Figure 17: Seismic geomorphology of a mixed-system offshore The Gambia, NW Africa. A)
1263 East-West two-way time seismic section with key stratigraphic surfaces, location shown in C. B)
1264 Enlarged two-way time seismic section of carbonate blocks observed in the deep-marine mixed-
1265 system. C) Depth structure map (contoured) with dip magnitude below of the diachronous
1266 regional composite unconformity surface displayed on seismic section A, showing the heavily
1267 canyonised carbonate escarpment margin, canyon flow pathways (dashed white lines),
1268 lithological contact between siliciclastic and carbonate subcrop (solid white line) and onlap
1269 surface (dotted white line). D & E) RMS amplitude maps extracted from a +/- 12 ms window
1270 around two Late Cretaceous horizons in the basin. Location of maps shown on C.

1271

1272

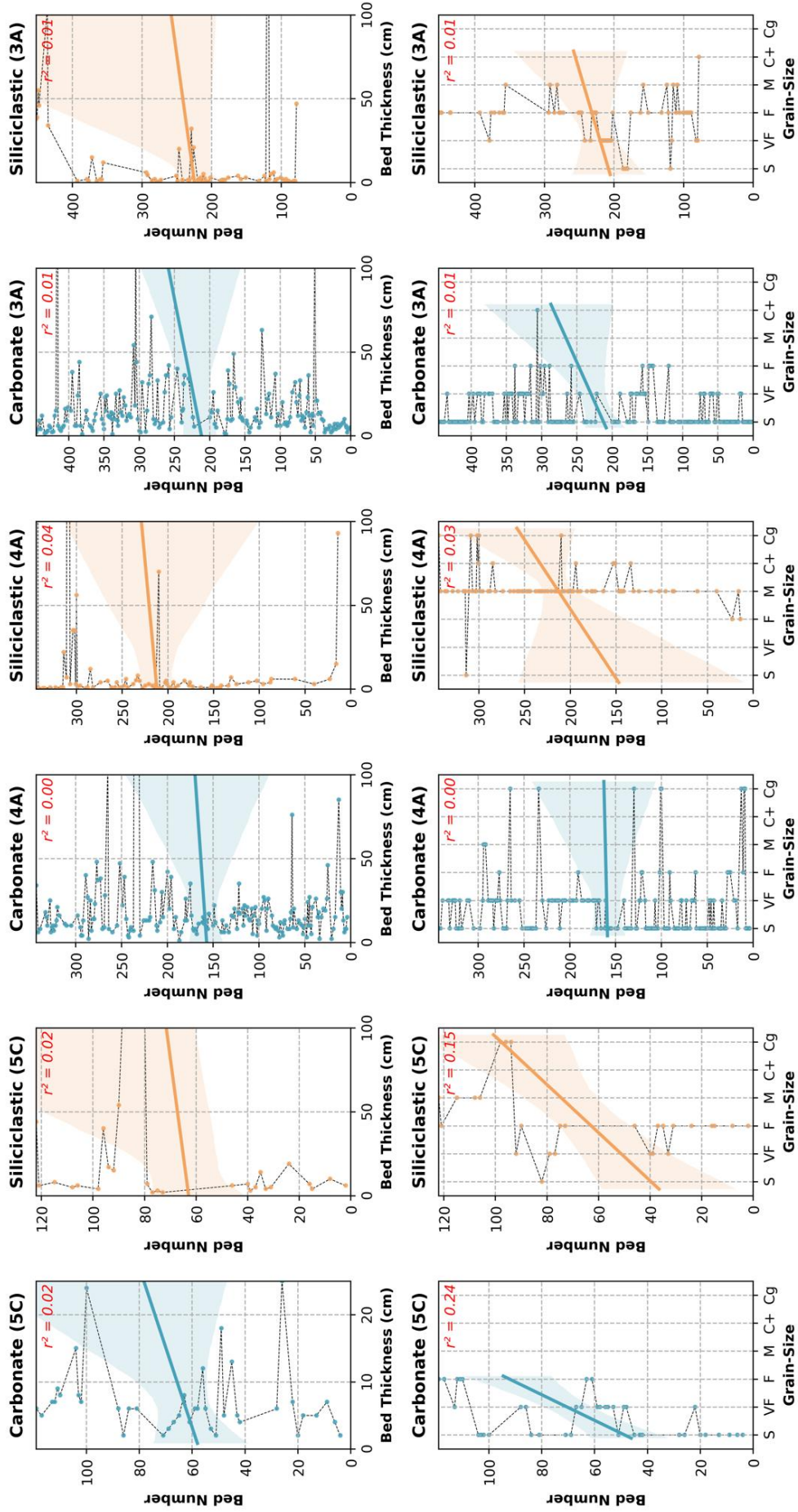
1273

1274

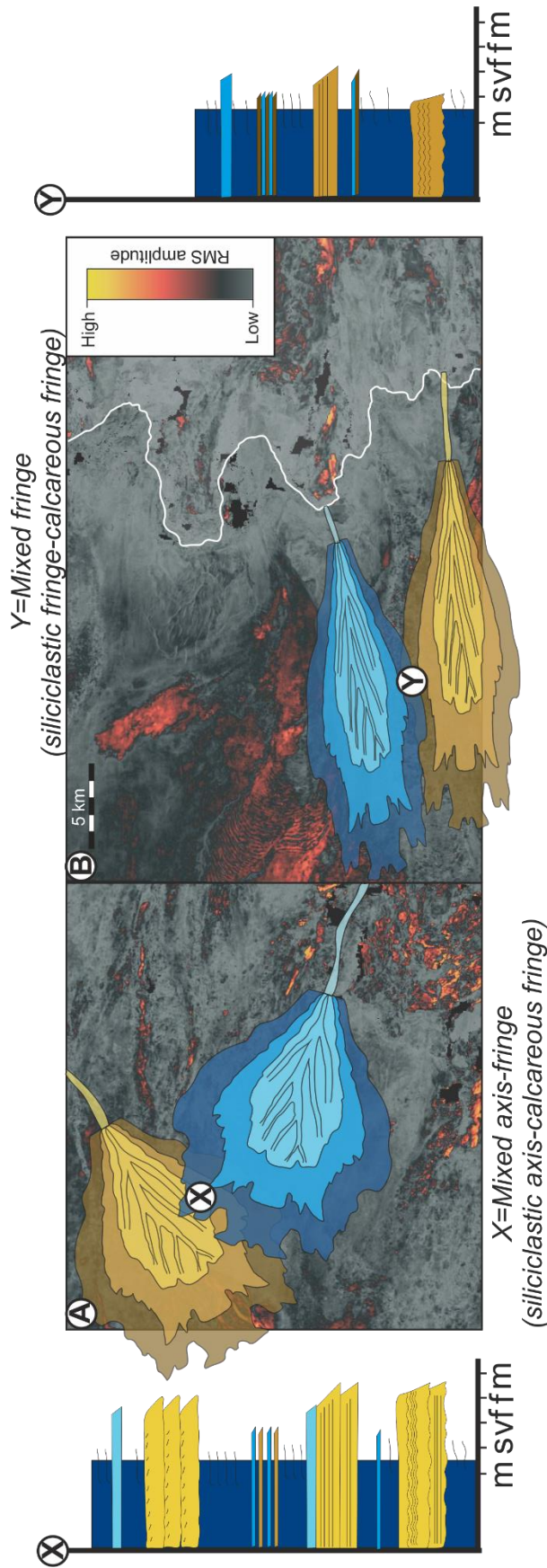
1275

1276

Carbonate/Siliciclastic Thickness & Grain-Size Trends



1278 Figure 18: Quantitative facies analysis for Coniacian-Maastrichtian stratigraphy. Logs are the
1279 same as Figures 8 and 10. 5C, 4A and 3A represent northern margin, axis and southern margin
1280 respectively. Each log is divided into carbonate and siliciclastic beds, and bed number is plotted
1281 against bed thickness (upper row) and grain size (bottom row). Lines indicate linear regression, r^2
1282 value is labelled in red, shading either side of the line indicates a 95% confidence interval for the
1283 linear regression (trend line). Low-no correlation is observed suggesting no stacking patterns or
1284 modulation of any stacking patterns by interaction of both systems, discussed in text.



1285
 1286
 1287
 1288

Figure 19: Schematic showing potential interactions of calcareous and siliciclastic lobes in mixed systems. A and B are RMS maps from Figure 17, which have been overlain by lobe complex

1289 geometries, as an interpretation based on seismic facies analysis and understanding of regional
1290 source area (see Casson et al. 2020). X and Y represent log/core through locations where the
1291 lobe complexes interact in A and B respectively. X crosses the lobe fringe of the calcareous
1292 system and the lobe axis of the siliciclastic system and Y crosses the lobe fringe of both systems
1293 resulting in a thinner and finer grained succession when compared to X. This variability
1294 highlights difficulties arising from exporting sub-environment terminology developed in
1295 siliciclastic systems (e.g. Pr elat et al. 2009) into mixed systems
1296